UNIVERSIDADE FEDERAL DO RIO GRANDE DO NORTE
INSTITUTO DO CÉREBRO
PROGRAMA DE PÓS-GRADUAÇÃO EM NEUROCIÊNCIAS
LABORATÓRIO DE NEUROFISIOLOGIA COMPUTACIONAL

BRYAN DA COSTA SOUZA

CARACTERIZAÇÃO DE CÉLULAS DE LUGAR NO HIPOCAMPO E SUAS RELAÇÕES COM OSCILAÇÕES DO POTENCIAL DE CAMPO LOCAL

(CHARACTERIZATION OF HIPPOCAMPAL PLACE CELLS AND THEIR RELATION TO LOCAL FIELD POTENTIAL OSCILLATIONS)

Natal - RN
2015

Bryan da Costa Souza

CARACTERIZAÇÃO DE CÉLULAS DE LUGAR NO HIPOCAMPO E SUAS RELAÇÕES COM OSCILAÇÕES DO POTENCIAL DE CAMPO LOCAL

(CHARACTERIZATION OF HIPPOCAMPAL PLACE CELLS AND THEIR RELATION TO LOCAL FIELD POTENTIAL OSCILLATIONS)

Dissertação apresentada ao Curso de Pós-Graduação em Neurociências, Instituto do Cérebro, Universidade Federal do Rio Grande do Norte, como requisito parcial para a obtenção do título de Mestre em Neurociências.

Orientador: Adriano Bretanha Lopes Tort

Natal - RN

2015

Catalogação da Publicação na Fonte Universidade Federal do Rio Grande do Norte – UFRN

Catalogação de Publicação na Fonte. UFRN - Biblioteca Setorial do Instituto do Cérebro

S719c Souza, Bryan da Costa.

.

Caracterização de células de lugar no hipocampo e suas relações com oscilações do potencial de campo local / Bryan da Costa Souza. - Natal, 2015.
76p: il.

Dissertação (Mestrado em Neurociências). Universidade Federal do Rio Grande do Norte. Orientador: Profº. Dr. Adriano Bretanha Lopes Tort.

.

1. Neurociências - Dissertação. 2. Células de lugar. 3. Campo receptivo de lugar. 4. Oscilações teta. 5. Oscilações gamma. 6. Hipocampo. 7. Córtex entorrinal I. Título

RN/UF/BSET/ICe CDU 612.8

UNIVERSIDADE FEDERAL DO RIO GRANDE DO NORTE

INSTITUTO DO CÉREBRO

PROGRAMA DE PÓS-GRADUAÇÃO EM NEUROCIÊNCIAS

ATA DA DEFESA DE DISSERTAÇÃO DE MESTRADO DO PROGRAMA DE PÓS-GRADUAÇÃO EM NEUROCIÊNCIAS DO INSTITUTO DO CÉREBRO DA UNIVERSIDADE FEDERAL DO RIO GRANDE DO NORTE

Aos treze dias do mês de março de dois mil e quinze, às 14h, no Auditório do Instituto do Cérebro da Universidade Federal do Rio Grande do Norte, reuniu-se em sessão pública a banca examinadora responsável pela avaliação da dissertação intitulada **"CARACTERIZAÇÃO DE CÉLULAS DE LUGAR NO HIPOCAMPO E DE SUAS RELAÇÕES COM OSCILAÇÕES DO POTENCIAL DE CAMPO LOCAL "** do mestrando **BRYAN DA COSTA SOUZA.** A Banca foi presidida pelo Profº Adriano Bretanha Lopes Tort - Presidente (UFRN), pelo Profº Diego Andres Laplagne- Examinador Interno (UFRN) e pelo Profº Olavo Bohrer Amaral – Examinador Externo (UFRJ). O Exame teve a duração de 1h30min e a Banca, após a apresentação formal do trabalho e argüição do mestrando, emitiu o seguinte parecer: TRABALHO COM MÉRITO DEMONSTRANDO QUE O CANDIDATO PREENCHE OS REQUISITOS considerando o aluno APROVADO (Aprovado/Reprovado). Nada mais havendo a tratar, foi lavrada a presente ata, que vai assinada pelos membros da banca examinadora e pelo mestrando.

BANCA DE DEFESA

Profº Adriano Bretanha Lopes Tort - Presidente (UFRN)_____

Profº Diego Andres Laplagne - Examinador Interno (UFRN)_____

Profº Olavo Bohrer Amaral – Examinador Externo (UFRJ)_____

Nota (0 a 10) 9

MESTRANDO

Bryan da Costa Souza_____

Natal, 13 de março de 2015.

BrainInstitute (UFRN)
Av. Nascimento Castro, 2155 – Natal – RN – Brazil
e-mail: pg@neuro.ufrn.br
phone: +55 (84) 3215-2709

Agradecimentos

Primeiramente à minha mãe, Ana, e ao meu pai, Carlson, que se dedicaram tanto para minha educação tradicional, moral e social.

Às minhas irmãs, Annie e Nicholy, por serem tão compreensivas e atenciosas comigo.

À Carol pelo companheirismo e amizade crescentes.

À Nati e Tonhaunm, pela amizade, carinho e conforto de sempre.

Aos meus amigos do laboratório de neurofisiologia computacional, cujas contribuições enriqueceram fortemente este trabalho: Hindiael, Arthur, Cesar, Vivi, Pavão, Lockman, Robson, Allan, Zé e China.

Aos meus amigos do ICe, uma segunda familia, que tornam os dias de trabalho tão suaves: Dudu, Ju, Kekinha, Melek, Dani, Aron, Heitor, Mayara, Débora, Jailson, Olguita, Johnny Dallas, Hjalmar, Daniel, Toppy, Sylpi, Kelly, Bruna, Giovanne, Dardo, Conde, FeiraGirl, Geissy e tantos outros.

Aos camaradas Aninha, Fujona, Phiphi, Pilha, Saroba, Bike, Menininha, Sininho, Muskito, Soneca, Carioca, Ninja, 18, Meg, Frajola, Piloto e Mestre Delicado pelo axé dentro e fora dos treinos.

Ao Instituto do Cérebro e todos os seus funcionários, em especial: Akaline, pela paciência eterna, e Sidarta, por me abrir as portas da neurociência.

À Olavo e Diego, pelas críticas e contribuições dadas para a melhoria deste trabalho.

À UFRN que é para mim uma segunda casa.

À CAPES pelo suporte financeiro.

Ao CRCNS, Gyorgy Buzsáki e seu laboratório por disponibilizarem os dados e acreditarem na ciência aberta.

Ao meu orientador, Adriano Tort, cujo esforço e empenho foi fundamental para a realização deste trabalho e, mais importantemente, minha formação contínua como cientista.

“Nenhum ser nos foi concedido. Correnteza apenas
Somos, fluindo de forma em forma docilmente:
Movidos pela sede do ser atravessamos
O dia, a noite, a gruta e a catedral

Assim sem descanso as enchemos uma a uma
E nenhuma nos é o lar, a ventura, a tormenta,
Ora caminhamos sempre, ora somos sempre o visitante,
A nós não chama o campo, o arado, a nós não cresce o pão

Não sabemos o que de nós quer Deus
Que, barro em suas mãos, connosco brinca,
Barro mudo e moldável que não ri nem chora,
Barro amassado que nunca coze

Ser enfim como a pedra sólido! Durar uma vez!
Eternamente vivo é este o nosso anseio
Que medroso arrepio permanece apesar de eterno
E nunca será o repouso no caminho”

Hermann Hesse, em ‘O jogo das Contas de Vidro’.

Resumo

Caracterização de células de lugar no hipocampo e de suas relações com oscilações do potencial de campo local.

As principais vias aferentes ao hipocampo vêm do córtex entorrinal e fazem parte de um *loop* que retorna ao entorrinal após passar pelo giro denteado, e pelas subareas do hipocampo CA3 e CA1. Desde a descoberta nos anos 50 de que o hipocampo está envolvido na formação de memórias, esta região vem sendo extensivamente estudada. Além desta função mnemônica, o hipocampo também está associado a navegação espacial. Em camundongos e ratos, células de lugar exibem um aumento da taxa de disparo relacionado à posição do animal. O local do ambiente onde uma determinada célula de lugar se ativa é chamado de campo de lugar. A taxa de disparo das células de lugar é máxima quando o animal está no centro do campo de lugar, e diminui a medida que ele se afasta desse ponto, sugerindo a existência de uma codificação espacial baseada em taxa de disparos. Entretanto, pesquisas prévias vêm mostrando a existência de oscilações hipocampais em múltiplas frequências e ligadas a diferentes estados comportamentais, e muitos acreditam que estas oscilações são importantes para uma codificação temporal. Em particular, oscilações teta (5-12 Hz) possuem uma relação espaço-temporal com as células de lugar conhecida como precessão de fase. Na precessão, a fase de disparos da célula de lugar muda gradualmente do pico de teta para o fundo e, posteriormente, para a fase ascendente, a medida que o animal atravessa o campo de lugar. Além disso, as teorias vigentes sugerem que CA1, a porta de saída do hipocampo, intermediaria a comunicação com o córtex entorrinal e CA3 através de oscilações em diferentes frequências chamadas, respectivamente, de gama alto (60-100 Hz; HG) e gama baixo (30-60 Hz; LG). Essas oscilações se relacionam com teta, estando aninhadas dentro de cada ciclo desta frequência mais lenta. Nesta dissertação, utilizamos dados disponibilizados online para fazer análises computacionais visando reproduzir resultados clássicos e recentes acerca da atividade das células de lugar no hipocampo de ratos em livre movimento. Em particular, nós revisitamos o debate sobre a relação da precessão de fase com variações na taxa de disparos e na posição do animal no campo de lugar. Concluímos que este fenômeno não pode ser explicado por nenhuma dessas variáveis sozinha, e sim pela interação entre elas. Nós também realizamos novas análises investigando as propriedades das células de lugar em relação às oscilações. Nós mostramos que o nível de modulação dos disparos por teta afeta apenas levemente a informação espacial contida nas células de lugar, enquanto a fase de disparo média não tem nenhuma influência na informação espacial. Também encontramos que as células de lugar estão moduladas por teta quando disparam fora do campo de lugar. Além disso, nossos resultados mostram que o disparo das células de lugar dentro do ciclo de teta segue os padrões de modulação de HG e LG por teta presentes nos potenciais de campo local de CA1 e córtex entorrinal. Por último, achamos um acoplamento fase-amplitude em CA1 associado apenas aos disparos dentro do campo de lugar na faixa de 40-80 Hz. Concluímos que o disparo de células de lugar está ligado a estados de rede refletidos no potencial de campo local e sugerimos que a atividade dessas células sejam interpretadas como um estado dinâmico ao invés de uma propriedade fixa da célula.

Palavras chave: Células de lugar, Campo receptivo de lugar, Oscilações teta, Oscilações gamma, Hipocampo, Córtex entorrinal.

Abstract

Characterization of hippocampal place cells and their relation to local field potential oscillations

The main inputs to the hippocampus arise from the entorhinal cortex (EC) and form a loop involving the dentate gyrus, CA3 and CA1 hippocampal subfields and then back to EC. Since the discovery that the hippocampus is involved in memory formation in the 50's, this region and its circuitry have been extensively studied. Beyond memory, the hippocampus has also been found to play an important role in spatial navigation. In rats and mice, place cells show a close relation between firing rate and the animal position in a restricted area of the environment, the so-called place field. The firing of place cells peaks at the center of the place field and decreases when the animal moves away from it, suggesting the existence of a rate code for space. Nevertheless, many have described the emergence of hippocampal network oscillations of multiple frequencies depending on behavioral state, which are believed to be important for temporal coding. In particular, theta oscillations (5-12 Hz) exhibit a spatio-temporal relation with place cells known as phase precession, in which place cells consistently change the theta phase of spiking as the animal traverses the place field. Moreover, current theories state that CA1, the main output stream of the hippocampus, would interplay inputs from EC and CA3 through network oscillations of different frequencies, namely high gamma (60-100 Hz; HG) and low gamma (30-50 Hz; LG), respectively, which tend to be nested in different phases of the theta cycle. In the present dissertation we use a freely available online dataset to make extensive computational analyses aimed at reproducing classical and recent results about the activity of place cells in the hippocampus of freely moving rats. In particular, we revisit the debate of whether phase precession is due to changes in firing frequency or space alone, and conclude that the phenomenon cannot be explained by either factor independently but by their joint influence. We also perform novel analyses investigating further characteristics of place cells in relation to network oscillations. We show that the strength of theta modulation of spikes only marginally affects the spatial information content of place cells, while the mean spiking theta phase has no influence on spatial information. Further analyses reveal that place cells are also modulated by theta when they fire outside the place field. Moreover, we find that the firing of place cells within the theta cycle is modulated by HG and LG amplitude in both CA1 and EC, matching cross-frequency coupling results found at the local field potential level. Additionally, the phase-amplitude coupling in CA1 associated with spikes inside the place field is characterized by amplitude modulation in the 40-80 Hz range. We conclude that place cell firing is embedded in large network states reflected in local field potential oscillations and suggest that their activity might be seen as a dynamic state rather than a fixed property of the cell.

Keywords: Place cell, Place field, Theta oscillations, Gamma oscillations, Hippocampus, Entorhinal cortex.

Abbreviations

CA1 – *Cornu Ammonis* area 1

CA2 – *Cornu Ammonis* area 2

CA3 – *Cornu Ammonis* area 3

CFC – Cross frequency coupling

CRCNS – Collaborative Research in Computational Neuroscience

DG – Dentate gyrus

EC – Entorhinal cortex

EC3 – Layer III of the entorhinal cortex

HG – High gamma

IFR – Instantaneous firing rate

LFP – Local field potential

LG – Low gamma

MI – Modulation index

MPVA – Mean phase vector angle

MPVL – Mean phase vector length

PSD – Power spectrum density

REM – Rapid eye movement

Index

1 Introduction

1 Introduction

1.1 The hippocampal formation

1.1.1 Role in memory formation

Since the famous study of Scoville and Milner (1957) we know that one major function of the hippocampus is the acquisition of certain types of memory. The hippocampus, along with the dentate gyrus (DG), entorhinal cortex (EC), subiculum, presubiculum and parasubiculum form the hippocampal formation, located in the medial temporal lobe (Andersen et al., 2006)[1]. Some of these areas are structured in a laminar profile similar to the one found in neocortex; they constitute a particular circuitry in which the EC mediates most of the inputs and outputs.

Scoville and Milner reported a medical case (patient H.M.) that presented partial, temporally graded, retrograde amnesia and a permanent inability of forming new episodic and event memories – also known as declarative memories – after a bilateral medio-temporal lobotomy. Although the surgical procedure was not restricted to both hippocampi (Scoville and Milner, 1957), later studies on human and animal lesions confirmed that this memory deficit is mainly related to damage of the hippocampus and other structures of the hippocampal formation (Mishkin, 1978; Victor and Agamanolis, 1990; Zola-Morgan et al., 1986, 1989).

The fact that mainly declarative memories are affected by hippocampal lesions helped to establish that memory is not a general and unique process (Squire, 1982; Squire and Zola-Morgan, 1991). Hippocampal loss, for example, does not impair the learning of skills or habits – classified as procedural memory (Corkin, 1968; Milner et al., 1968). Similar results in animal studies corroborate the separated

[1] There is no consensus of which areas do form the hippocampus. Herein we use the definition suggested by Andersen and colleagues in the *Hippocampus book* which consider that the hippocampus has only three subdivisions: CA1, CA2 and CA3. In this definition, the dentate gyrus is part of the hippocampal formation together with other areas and the hippocampus itself.

memory system hypothesis (Eichenbaum et al., 1986, 1989; Morris et al., 1982; O'Keefe and Nadel, 1978; Olton et al., 1978a; Zola-Morgan and Squire, 1984).

Because hippocampal lesions partially affect recent memories but not old ones, another important aspect of (declarative) memories was clarified: although the hippocampus is needed to form new memories, they are not permanently stored there (Zola-Morgan and Squire, 1990). In fact, long-term declarative memories, as well as working memory, seem to be encoded in cortical regions (Fuster, 2001). Together, this knowledge has led to the origin of current theories that state that short-term memory initially represented in the cortex may also become coded by the hippocampus. These representations would then gradually migrate back to neocortex through a consolidation process, forming long-term memories (Eichenbaum, 2000a) (alternatively, the multiple trace theory states that even long-term memory representations are partially encoded at the hippocampus, see Nadel and Moscovitch, 1997).

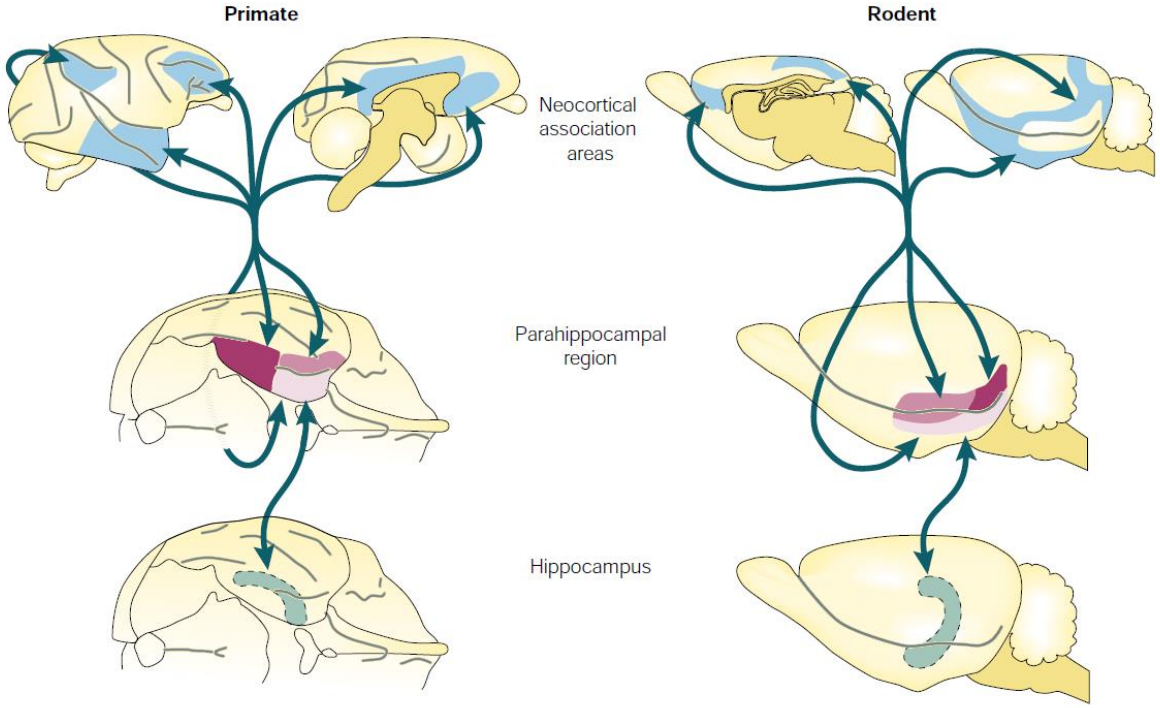

Figure 1.1 – Encoding and retrieval of hippocampal dependent memories in the primate and rodent brains. Information from neocortical areas reaches the parahippocampal regions and is stored in the hippocampus. Then, memory representations in the hippocampus gradually migrate to the neocortex through the reverse way for a more permanent storage. Adapted from Eichenbaum (2000a).

The anatomical characteristics of the hippocampus and experimental evidence (Eichenbaum, 2000a; Squire and Zola-Morgan, 1991) suggest that this migratory process is mediated by the parahippocampal region, formed by the perirhinal, postrhinal and entorhinal cortices, which are responsible for most of the cortical input to the hippocampus (Figure 1.1). The perirhinal and postrhinal cortices receive inputs from unimodal and multimodal cortical areas and project to the entorhinal cortex (Witter, 1992). The entorhinal cortex, in turn, projects to the hippocampus and dentate gyrus, acting as a convergence site from the neocortex. From the hippocampus, projections reach back to the same neocortical areas in the opposite direction, going from the entorhinal cortex to the perirhinal and postrhinal cortices, and from there to the neocortex (Eichenbaum, 2000a; Squire and Zola-Morgan, 1991). As the entorhinal cortex is the main gateway for information to enter and leave the hippocampus, this dissertation focus on it among the other parahippocampal regions.

1.1.2 Anatomical characteristics

The entorhinal cortex (EC) is commonly divided in six layers: four cellular layers (II, III, V and VI) and two acellular layers (I and IV). The most superficial layers (II and III) receive cortical inputs coming from perihinal and postrhinal cortices and send projections to dentate gyrus (DG) and hippocampus, while the deepest layers (IV, V and VI) receive inputs from the hippocampus and send afferents to the neocortex.

Briefly (see Andersen et al., 2006 for details), afferent projections from layer II of the EC reach one of the three DG layers, the molecular layer, which is occupied mostly by dendritic trees and axon terminals. This layer also receives projections from mossy cells in both ipsi- and contra-lateral polymorphic layers of the DG. The granule cell layer, the middle layer of the DG, receives GABAergic and cholinergic inputs from basket cells at the ipsilateral polymorphic layer and from septum, respectively. The axons from the granule cells form the mossy fibers, the only projections that leave from the DG to the hippocampus which also form synapses with the mossy cells in the polymorphic layer.

The hippocampus is divided in three different sub-regions called *Cornu Ammonis* (CA) areas: CA1, CA2 and CA3. Each of them presents a laminar profile formed by 5 or 4 strata, as shown in Figure 1.2. The mossy fibers enter the hippocampus through CA3, where they project onto the stratum lucidum. CA3 then projects to CA1 through the Schaffer collaterals. CA3 and CA2 have very similar connectivity patterns except for the absence of the stratum lucidum in CA2. They are characterized by the presence of recurrent connections in strata oriens and radiatum and of external inputs from EC layer II arriving at stratum lacunosum-moleculare. They also receive inputs from the septum and amygdaloid complex.

The Schaffer collaterals leave from CA3 and CA2 to strata radiatum and oriens in CA1. CA1 receives similar external inputs from the septum and amygdaloid complex, and, in addition, it receives projections from EC layer III (rather than II in CA2/CA3) and sends projections to the deepest layers of the EC: IV, V and VI. CA1 also projects to the subiculum and has reciprocal connections with the perirhinal cortex.

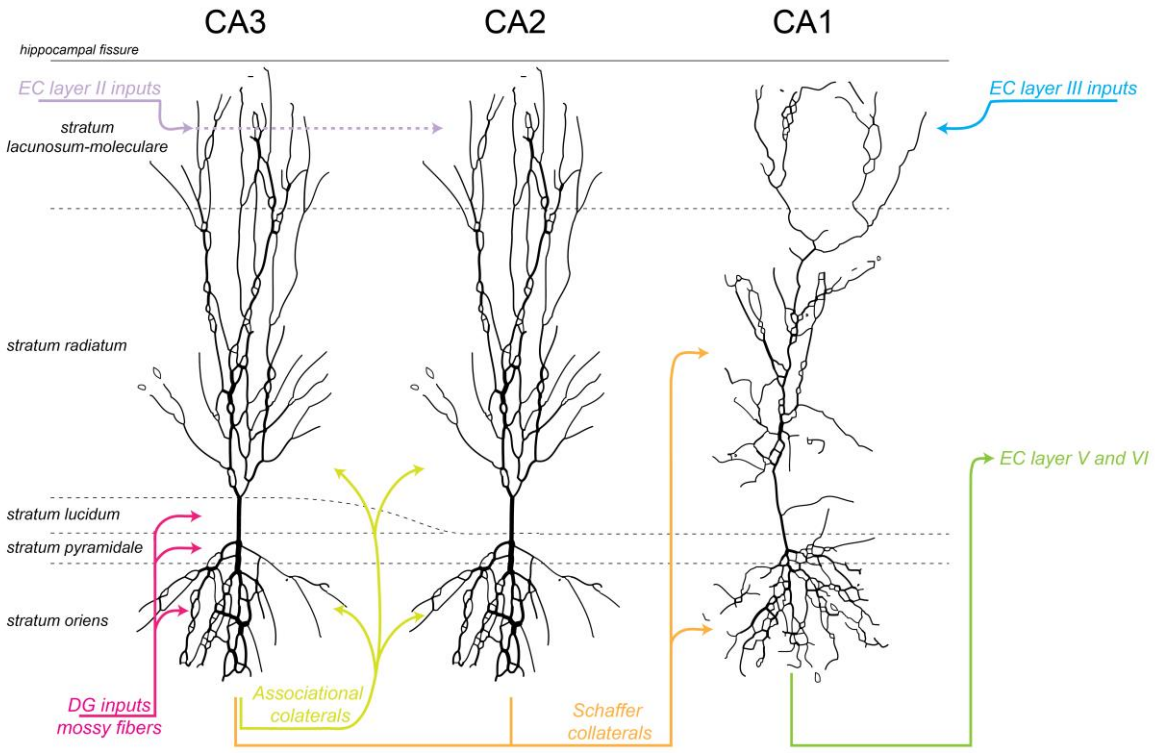

Figure 1.2 – The main hippocampal projections. DG mossy fibers reach CA3 at the strata lucidum, pyramidale and oriens, while projections from EC layer II reach the stratum lacunosum-moleculare. CA3 and CA2 receive similar projections except for the absence of DG inputs in CA2. They are characterized by recurrent connections in strata oriens and radiatum. From CA2/CA3 the Schaffer collaterals projects to strata oriens and radiatum in CA1. Additionally, CA1 receives afferents from EC layer III. Finally, CA1 sends projections to EC layers V and VI.

1.1.3 Hippocampal rhythms

Many structures in the brain present a cytoarchitecture in which groups of cells are organized in a same orientation. Because of this, inward and outward currents of nearby cells can generate a resultant potential in a non-destructive interference pattern. This potential, known as local field potential (LFP), is believed to indicate the degree of synchrony of neurons in the local circuits (Buzsáki et al., 2012). Although the LFP is generated by the joint activity of these neurons, we can also investigate the activity of a single neuron in relation to the LFP and, thus, to the local population. For example, the LFP can synchronize the activity of distant neurons (Lubenov and Siapas, 2009). For practical purposes, we consider the LFP activity as independent from spiking activity.

In 1954, the classical work by Green and Arduini showed that a 5-7 Hz rhythm appeared in the LFP of the rabbit's hippocampus when the animal was alert (Green and Arduini, 1954). Since then, this rhythm – termed theta oscillation – was studied in the rat, mouse, cat, monkey and other mammals and has been associated with a variety of behaviors (see Figure 1.3; Buzsáki, 2005; Winson, 1972). Although there is still no consensus about the role of theta, this rhythm is believed to participate in arousal and other cognitive process such as decision making (Belchior et al., 2014; Bland and Oddie, 2001; Tort et al., 2009).

Theta in the hippocampus can be of two types: a slower theta (4-7 Hz) that is abolished by atropine sulfate, and a faster theta (7-12 Hz) that is insensitive to atropine but strongly associated with locomotion (Kramis et al., 1975). This dichotomy was later found to represent two different theta generators, one – atropine-sensitive – originated from CA3 recurrent connections and other – atropine-resistant – mediated by NMDA receptors from EC inputs to the hippocampus (Buzsáki, 2005).

In the rat other robust behavior landmarks for the presence of hippocampal theta (5-12 Hz) are voluntary movement and rapid-eye movement (REM) sleep (Vanderwolf, 1969). In fact, theta oscillations were found to be important for spatial learning and navigation (Winson, 1978) and to correlate with the animal's speed (Sławińska and Kasicki, 1998).

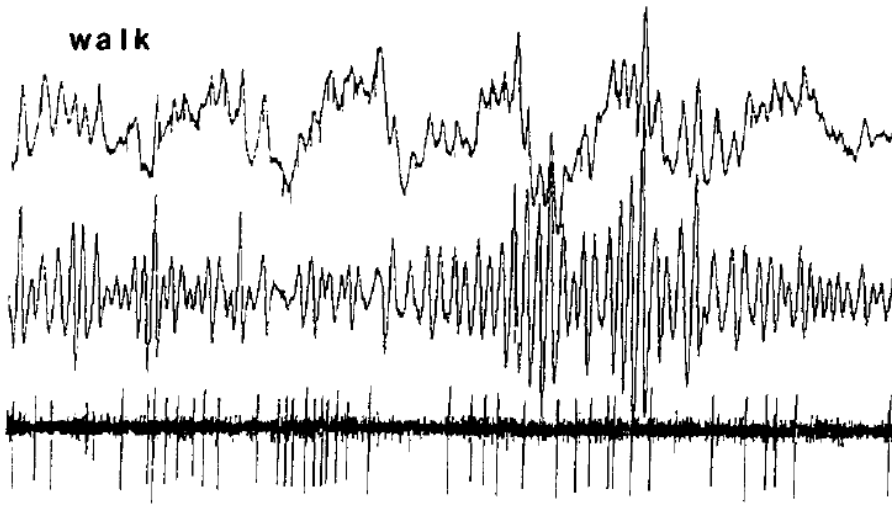

Figure 1.3 – Theta and gamma oscillations in the hippocampus of the rat during walking. Shown are theta and gamma oscillations in an LFP (top), gamma-filtered LFP (middle) and multiunit activity (bottom). Adapted from Bragin and colleagues (1995).

Another important brain rhythm in the brain is the gamma oscillation, a fast rhythm in the 30-100 Hz range (Figure 1.3). This rhythm is associated with perceptual responses in many cortical areas of the brain (Brosch et al., 2002; Desmedt and Tomberg, 1994; Freeman, 1978; Gray and Singer, 1989; Lebedev and Nelson, 1995) and, thus, is believed to play an important role in neuronal synchronization and cortical information process (Fell et al., 2003). Gamma is also associated with temporal expectation and focused attention (Desmedt and Tomberg, 1994; Fell et al., 2003; Fries et al., 2001; Gruber et al., 1999; Lima et al., 2011).

Gamma oscillations are found in DG and CA1 and are thought to arise from two different sources: external EC inputs and CA1-CA3 hippocampal connections (Bragin et al., 1995; Csicsvari et al., 2003). The EC associated gamma is strongest in the hilar region of the DG and oscillates around ~80 Hz. On the other hand, gamma from the CA3 generator is a slower oscillation (~40 Hz) and is most evident in CA1 after EC lesions when the DG-induced gamma virtually disappears (Bragin et al., 1995; Csicsvari et al., 2003). These two different gammas are usually classified as high gamma (~80 Hz; HG) and low gamma (~40 Hz; LG).

It is believed that brain oscillations can interact through different forms of cross-frequency coupling (CFC). Similar to the AM or FM radio waves, this mechanism could subserve to exchange information between distant areas. In fact, CFC patterns, and specially phase-amplitude CFC, were found in many species (Bragin et al., 1995; Buzsáki et al., 2003; Canolty and Knight, 2010; Jensen and Colgin, 2007) and have been associated to behaviors such as decision making and working memory (Axmacher et al., 2010; Tort et al., 2008, 2009). In the hippocampus, CFC occurs between theta and gamma oscillations, in which gamma amplitude is modulated by the phase of theta (Bragin et al., 1995). These rhythms are also related in other ways; for example, gamma activity is larger during theta associated behaviors such as REM sleep, exploration and movement and its frequency seems to covary with theta frequency (Bragin et al., 1995).

Because LG and HG represent two gamma generators and have amplitude peaks in different theta phases (Colgin et al., 2009; Schomburg et al., 2014), it has been hypothesized that CA1 gamma pattern could alternate between HG and LG to emphasize EC and CA3 communication, respectively (Figure 1.4) (Bieri et al., 2014; Colgin et al., 2009). In the first case, gamma would represent the sensory information

arriving in the hippocampus, while in the second gamma would represent stored information (Colgin et al., 2009). This hypothesis is supported by the anatomical configuration of CA1 inputs and the laminar pattern of HG and LG occurrence (Scheffer-Teixeira et al., 2012; Schomburg et al., 2014).

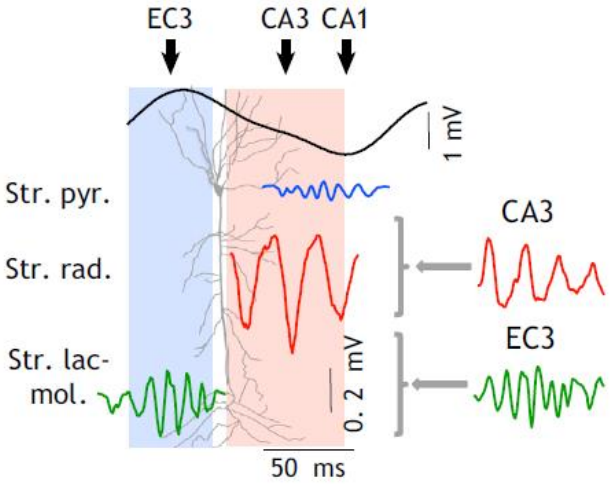

Figure 1.4 – Model of EC layer III (EC3) and CA3 interactions with CA1. EC3 inputs would arrive in CA1 through high gamma (HG) oscillations nested near the peak of pyramidal theta. In the descending phase of theta, low gamma (LG) oscillations would favor interactions with projections coming from CA3. Finally, the fast oscillations nested in the theta valley would arise from the activity of CA1 itself. Adapted from Schomburg and coleagues (2014).

1.2 Place cells

In 1971, O'Keefe and Dostrovsky found a strong link between the rat hippocampus and spatial navigation: hippocampal units that increased the firing rate whenever the animal was in a specific place of the environment (O'Keefe and Dostrovsky, 1971). Such units were termed 'place cells' and the area in which they had increased activity the 'place field'. Because place cell activity can be dissociated from other behaviors (Muller et al., 1987; Olton et al., 1978b), it was hypothesized that they were part of a spatial representation system in the hippocampus – the cognitive map theory (O'Keefe and Nadel, 1978). Experimental evidence corroborating this theory showed that the hippocampus is important in spatial learning and navigation (Morris et al., 1982; O'Keefe et al., 1975). Additionally, later studies found cells with different spatial correlates in other regions of the

hippocampal formation: the head direction cells, in the postsubiculum (Ranck Jr, 1984; Taube et al., 1990) and the grid cells, in the EC (Hafting et al., 2005).

Place cells are mostly principal cells of CA1 and CA3 (Fox and Ranck Jr, 1981). They seem to be anchored by more than a single cue in the enviroment (O'Keefe and Conway, 1978) and can be stable even after the removal of all spatial cues or in darkness (Muller and Kubie, 1987; O'Keefe and Speakman, 1987; Quirk et al., 1990). There is no topographic representation between the anatomical location of place cells and their place field location (O'Keefe et al., 1998; Redish et al., 2001), although the average place field size increases from dorsal to ventral hippocampus (Jung et al., 1994).

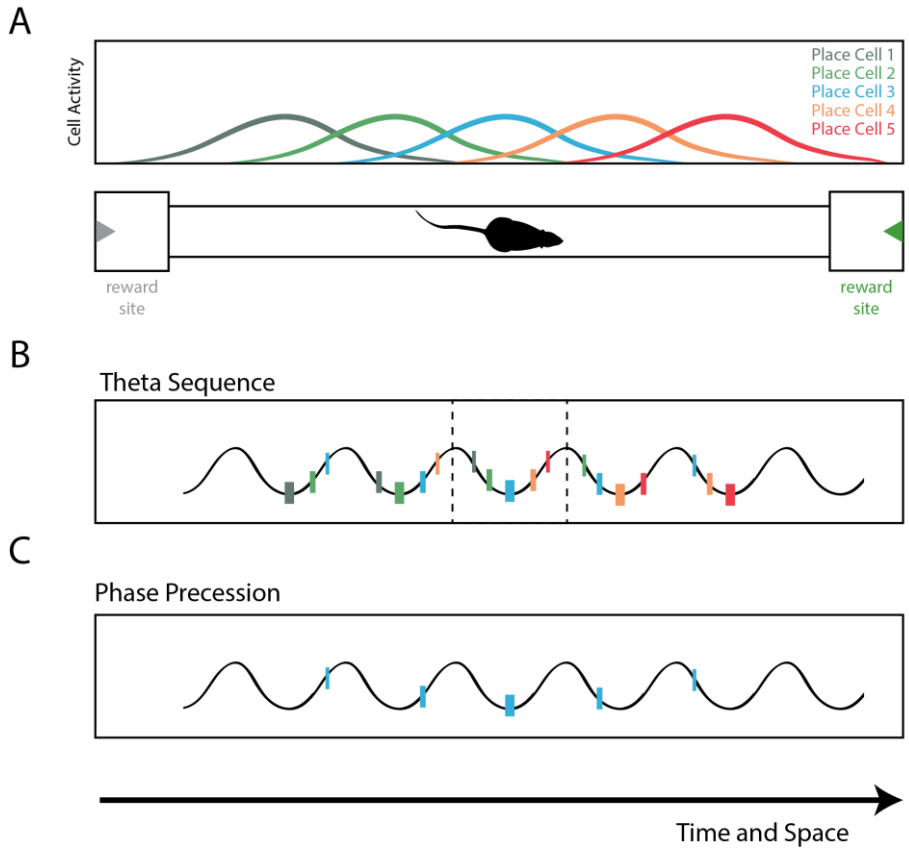

Figure 1.5 – Scheme of place cell phase precession. (A) Overlapping place fields are activated sequentially as the rat runs through the linear track. (B) Place cells spike maximally at the theta valley when the animal is at the place field center (firing rate is represented by the thickness of vertical traces). (C) When the animal is at the beginning of the place field the cell tends to fire at the theta peak. As the animal crosses the field the firing phase precess so that most of spikes in the center and end of the place field occur at the theta trough and descending phase, respectively.

Because hippocampal theta rhythm is important for spatial memory (Winson, 1978), it could be expected that this oscillation is related to place cells. Almost 20 years after the discovery of place cells, O'Keefe and Recce (1993) found that the theta phase of place cell firing covaries with the position inside the place field. This phenomenon was called phase precession, because the firing phase precesses as the animal crosses the place field (O'Keefe and Recce, 1993). Specifically, when the animal enters the place field, spikes tend to occur at the descending phase of theta (recorded in the pyramidal cell layer). As the animal approaches the place field center and leaves the place field, the spiking phase precesses to the trough and to the ascending phase of theta, respectively (see Figure 1.5 and Figure 1.6). Thus, the place cells oscillate in a faster frequency than the LFP theta when the animal crosses the place field (Geisler et al., 2007, 2010; O'Keefe and Recce, 1993).

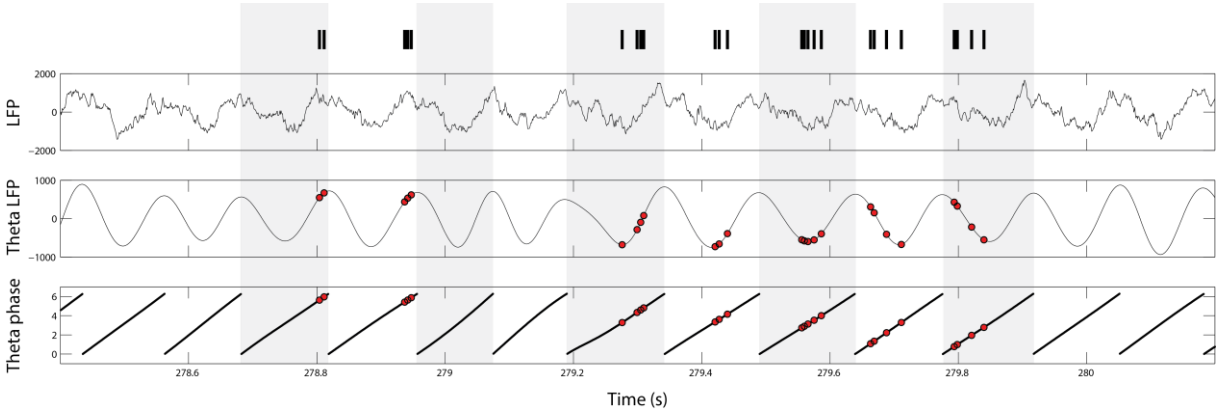

Figure 1.6 – Example of single trial phase precession. Shown are traces for raw and theta-filtered (5-12 Hz) LFP, along with instantaneous theta phase and spike times from a place cell while the animal crosses its place field. Note in the red dots that the spikes progressively move from the peak to the ascending phase, the trough and the descending phase (figure made from the actual dataset analyzed in this dissertation).

The phase precession phenomenon put in perspective the nature of the possible mechanisms underlying spatial representation. If on one hand the firing properties of place cells allow the spatial information to be decoded from firing rates, on the other hand phase precession enables this information to be also decoded from spike timing. Whether the brain uses both, one or none of these mechanisms remains an open question, despite the efforts on modeling and investigating their properties (Harris et al., 2002; Huxter et al., 2003; Mehta et al., 2002).

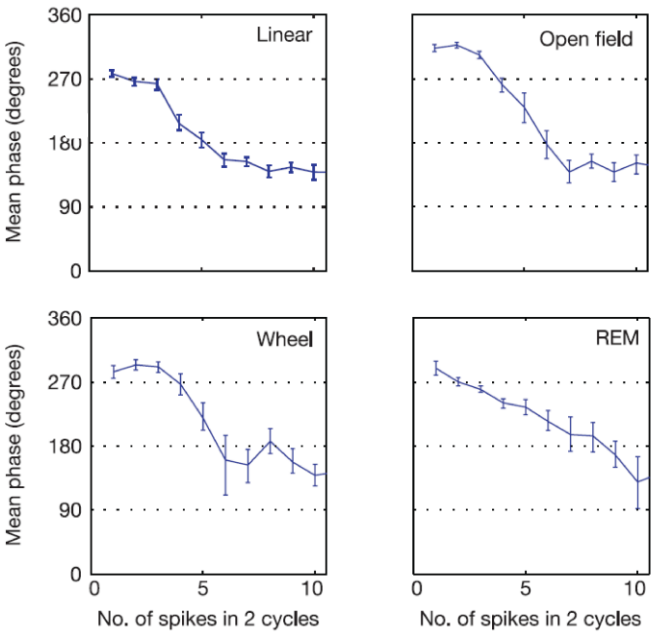

Figure 1.7 – Spiking theta phase correlates with instantaneous firing rate (IFR). Shown are circular mean phase of spiking and 95% confidence intervals for different values of IFR during different tasks: a linear track, an open field, a running wheel, and during REM sleep. Recordings were made from fifteen male rats. Adapted from Harris and colleagues (2002).

Harris and colleagues (2002) proposed that the phase precession was an intrinsic property of pyramidal cells, which occurred whenever the neuron had a burst of activity. They showed that the preferred spike phase of place cells varied with the increase of firing rate not only when the animal was crossing the place field, but in other cases such as in REM sleep or in a running wheel (Figure 1.7). This view was later criticized by Huxter and colleagues (2003) who found that the firing phase inside the place field was better correlated with position than with either firing rate or time (Figure 1.8).

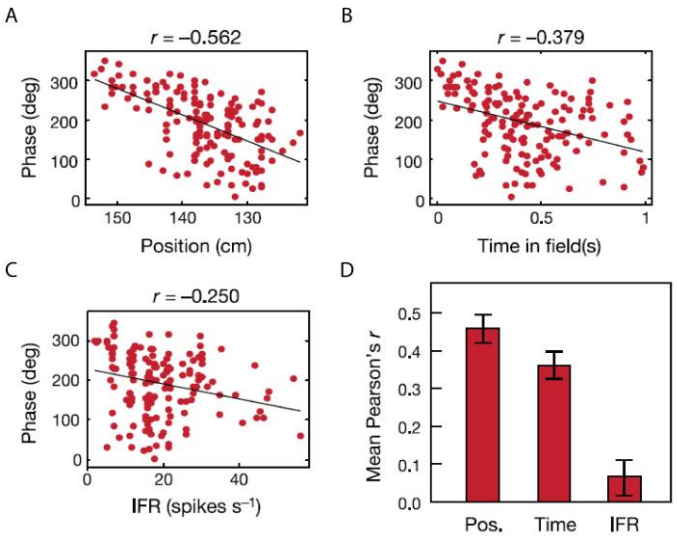

Figure 1.8 – Correlation of spiking theta phase with different variables. (A), (B) and (C) show the spiking phase of one place cell versus position, time and IFR, respectively. (D) shows the mean Pearson's r across place cells (error bars represent ± SEM). Recordings were made from nine Lister rats. Adapted from Huxter and colleagues (2003).

They defended that firing phase and rate are independent and can work as mechanisms encoding different variables, respectively, position and speed inside the place field. Only in 2014, however, an approach controlling both position and rate was used to investigate the joint dependency of place cell firing phase (Cei et al., 2014). They showed that, for a same instantaneous firing rate (IFR), the firing phase varies as a function of position, as shown by Huxter and colleagues. On the other hand, for a same position the firing phase varies as a function of IFR, as shown by Harris and colleagues (2002) (Figure 1.9). Thus, the firing phase of place cells seems to depend on both position and firing rate (Cei et al., 2014).

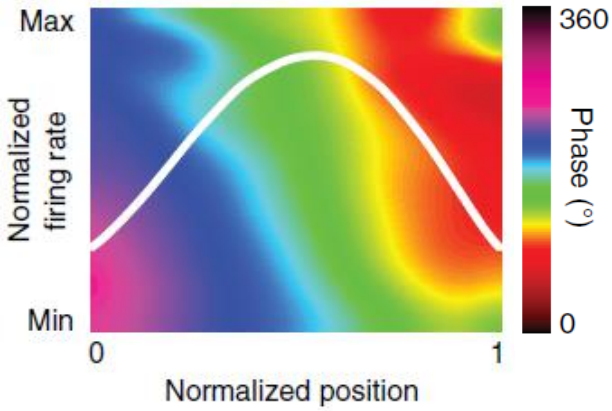

Figure 1.9 – Phase precession dependency on rate and position. Mean phase for different combinations of rate and position for the pool of place cells. White line represents the mean firing rate over the place field. Note the absence of vertical or horizontal stripes in the color map, indicating that phase is dependent on both axes. Adapted from Cei and colleagues (2014).

The discovery of place cells led to the hypothesis that the hippocampus subserves the creation of a spatial representation map (O'Keefe and Dostrovsky, 1971; O'Keefe and Nadel, 1978). However, this hypothesis does not replace other known functions of hippocampus, such as its role in non-spatial memory (Bunsey and Eichenbaum, 1996; Zola-Morgan et al., 1986). Evidence showing that place cells can have different activation at the same place but in different contexts supports the idea of place cells representing a conjunction of behavior and place (Eichenbaum, 2000b; Eichenbaum et al., 1999), and might allow one to understand the theories of the cognitive spatial map and the hippocampal memory system as one single view. Whether place cells are also involved in non-spatial memory when they are not encoding the animal's position is still an open question.

In summary, as reviewed above, the hippocampus is involved in some types of memory formation and spatial representation. Moreover, the hippocampus is part of a peculiar circuitry involving the EC and other structures of the hippocampal

formation. In particular, CA1 is believed to communicate with EC and CA3 through different oscillations, respectively, HG and LG, thought to be involved in memory processes. However, there is a paucity of studies trying to understand relations among LFP oscillations at different gamma frequencies and place cell activity, which could help understand the link between the spatial and mnemonic functions of the hippocampus.

1.3 On the present work

In this dissertation we characterize place cell activity using two main approaches. The first one concerns the replication of classical and recent results, and in the second one we perform novel exploratory analyses to investigate the interaction of place cells with LFPs. In particular, we study the relation between place cell activity and the theta phase coupling with both HG and LG amplitude. We also explore potential differences in the activity of place cells across and outside the place field.

2 Objectives

2 Objectives

Hippocampal place cells were described more than 40 years ago (O'Keefe and Dostrovsky, 1971). It is thus fair to say that the study of place cells is an old, yet still active[2], field of Neuroscience.

The first objective of the present dissertation was to replicate a myriad of characteristics of place cells that have been described over the last decades. Although time consuming, this step was crucial for consolidating in the author practical insights on the behavior of these cells[3]. The replication of classical findings also served as a positive control for the quality of the analysis algorithms, which were programmed from scratch. The second objective was to revisit the debate on the dependency of firing phase ("phase precession") on both position and firing rate, which was sparked by influent papers like those of Harris and colleagues (2002) and Huxter and colleagues (2003), and which seemingly was only recently solved by means of new analysis techniques (Cei et al. 2014). The third objective was to perform new analyses of place cell activity, which included looking for potential dependencies of place information on theta modulation of spikes and firing rate, and the study of place cell behavior inside vs. outside the place field. Finally, the fourth objective of this dissertation was to try to link the activity of place cells with gamma oscillations, so as to search for evidence of the alleged importance of gamma in CA1-EC communication.

[2] Noteworthy, in December 2014 John O'Keefe was awarded the Nobel Prize in Physiology or Medicine for his seminal discovery of hippocampal place cells.This nomination coincided with the final stage of the research done in this dissertation.

[3] Despite the fact that more than 40 years have passed, it is worth mentioning that – to the best of our knowledge – to date no laboratory in Brazil has produced a paper in this well-established field of research.

In summary and in bullet points, the specific objectives of this work were:

1. To replicate classical findings regarding place cell activity (e.g., spatial information content, place field shape, unidirectionality in linear mazes, phase precession);

2. To explore possible dependencies of spatial information on theta modulation of spikes;

3. To revisit the dependency of firing phase on position and firing rate;

4. To explore place cell activity inside and outside the place field concerning:
   (1) The frequency of spiking activity and its relation to the LFP;
   (2) Modulation by theta phase;

5. To explore the relation of place cell activity with gamma oscillations in the hippocampal-entorhinal circuit.

3 Materials and Methods

3 Materials and Methods

3.1 The open source dataset

In recent years, the sharing of data, codes and tools has been constantly increasing. Open Science, as it is called, brings clarity and efficacy to science publication as the published results can be more easily replicated and reproduced. In this study, we used a shared dataset from the Collaborative Research in Computational Neuroscience (CRCNS; https://crcns.org/), which is freely available for download online (Mizuseki et al., 2013, 2014). This dataset contained LFPs and spike times and waveforms of electrodes in CA1, CA3, EC and/or DG of 11 Long-Evans rats and was contributed by the Gyorgy Buzsáki Lab, now at New York University (the dataset was collected at Rutgers University). Below we first describe the part of the online dataset used in this work (we restricted our analyses to animals in the linear track with recordings in both the EC layer III (EC3) and CA1). The description includes information about the animal's surgery and behavior, the data acquisition and the histological verification of recordings. These were done in Buzsáki's Lab. In the next section we focus on the analyses performed by us..

3.1.1 Animals and surgery

Three male Long Evans were implanted with 4-shank silicon probes in the right dorsocaudal medial EC and 4-shank or 8-shank silicon probes in the right dorsal hippocampus during isoflurane anesthesia (Figure 3.1). Each silicon probe was attached to a micromanipulator and was independently moved through the days of recording. The EC probe was positioned in order to record from different layers of EC while the hippocampal probe was parallel to the septo-temporal axis, allowing recordings from pyramidal layer of CA1, CA3 or the granule cell layer of DG (see Figure 3.2). The shanks were interleaved by 200 μm and each of them had 8 contacts (160 μm^2 each site; 1-3 MΩ impedance) separated by 20 μm (Fujisawa 2008), providing a recording grid in a plane. All protocols were approved by the Institutional Animal Care and Use Committee of Rutgers University.

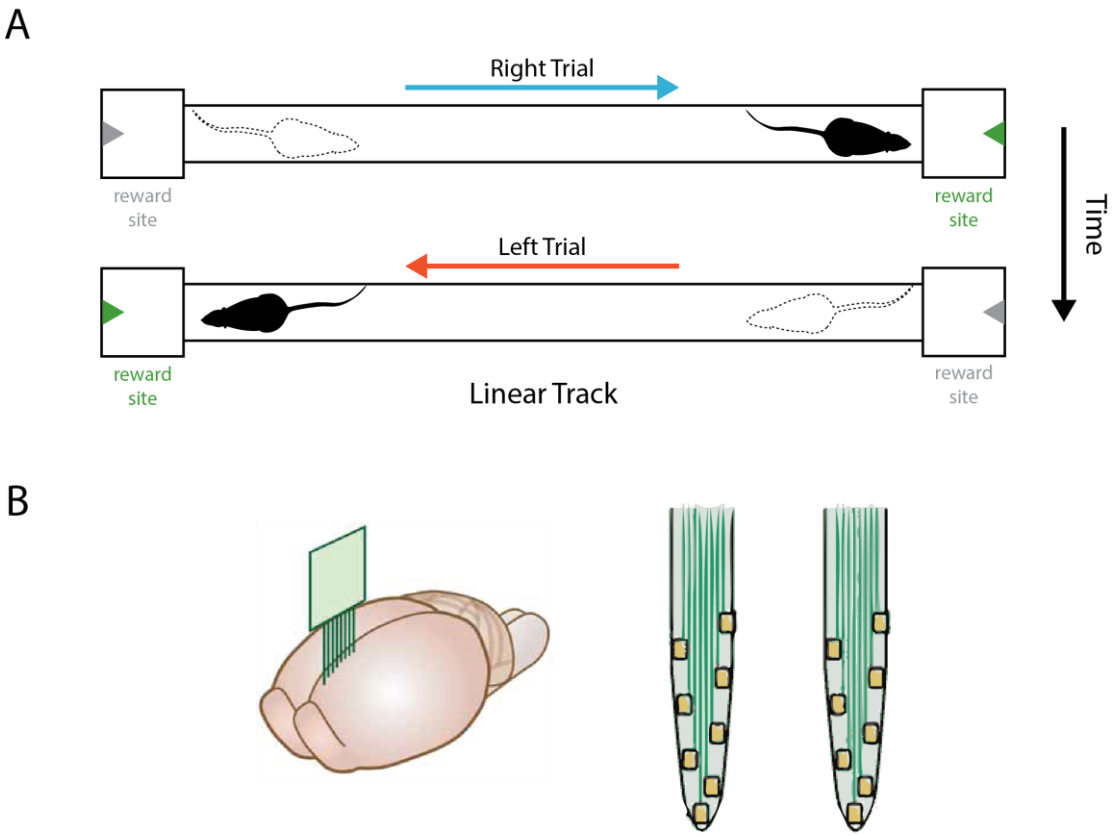

Figure 3.1 – Scheme of behavioral task and electrode recordings. (A) The rat had to alternate between the ends of a linear track in order to receive reward. (B). 4-8 Probes were implanted in the hippocampus. Adapted from Fujisawa and colleagues (2008).

3.1.2 Histological identification of recording sites

After the period of experiments the animals were anesthetized and perfused in saline and formalin solution. Their brains were cut into 100 µm slices and tissue sections mounted on slides for Nissl staining. The identification of the silicon probe tracks was done with the help of a fluorescent dye applied at the back of the shanks before implantation and a DC current applied 1-2 days before sacrifice (Figure 3.2). The position of the silicon probes in each session were then estimated using the LFP patterns and the distance the probe was moved between sessions, in addition to the histological data.

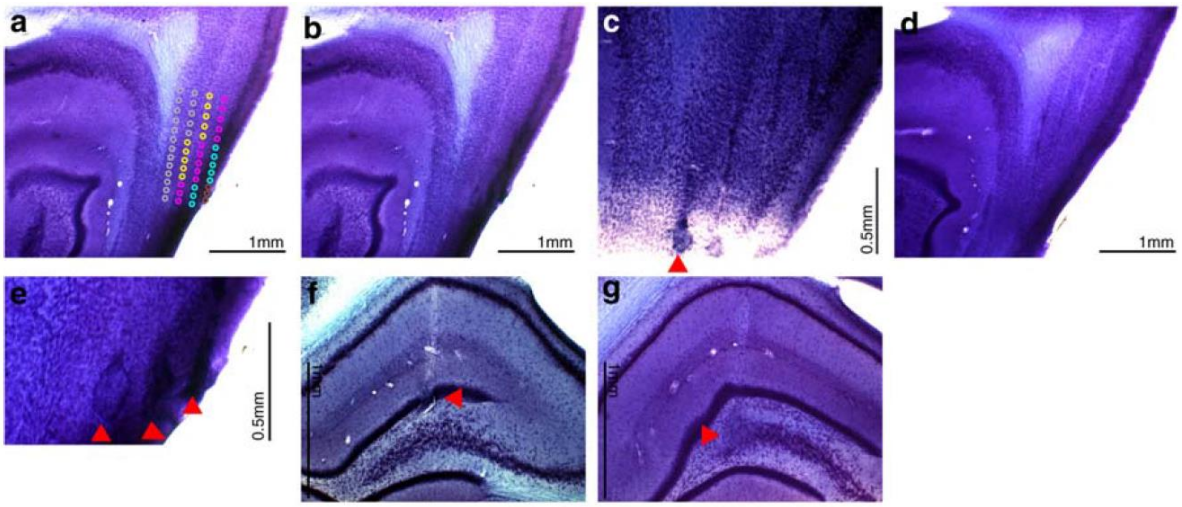

Figure 3.2 – Histological verification of recording sites in the EC and hippocampus. Sagittal sections from EC (a-e) and coronal sections from hippocampus (f-g). Circles in (a) show inferred position of electrodes for different consecutive sessions (color code for different layers); (b) shows the same section in (a) without the circles; (c) and (d) show sections adjacent to (a), arrowhead indicate the electrolytic lesion; (e) is a higher magnification of (b) where we can see the three other lesions (arrowheads); (f) and (g) show the electrolytic lesions of CA3 and DG, respectively. Adapted from Mizuseki and colleagues (2009).

3.1.3 Behavioral task and data collection

Approximately one week after surgery, the animals were put in a 250 cm linear maze for the recording sessions. They were water deprived for 24 h before the sessions and had to go back and forth to receive 30 µl of water at the ends of the apparatus (Figure 3.1). The neurophysiological signals were amplified 1.000X, band pass filtered (1 Hz-5 kHz) and acquired on a 128-channel DataMax system (DataMax system, RC Electronics) at 20 kHz or a NeuraLynx at 32,552 kHz (NeuraLynx system). The wideband signals were downsampled to 1250 Hz (or 1252 Hz in the case of NeuraLynx) to get the LFPs. The raw signal was high-pass filtered at 800 Hz and a threshold (~7 standard deviations above the mean) was set to get the spikes (Figure 3.3). Spike waveforms were sorted using KlustaKwik (Harris et al., 2000) and manually adjusted with “Kluster” package. The refractory periods and the cluster boundaries were used to guarantee only well-defined units were used in the analysis (Harris et al., 2000). In cases where the electrodes were not moved between two sessions in a same day, the waveforms were concatenated to sort the spikes. The

behavior of the animal was video recorded at 39.06 Hz. Two LEDs in the head of the rat were used to get the animal's position along the sessions.

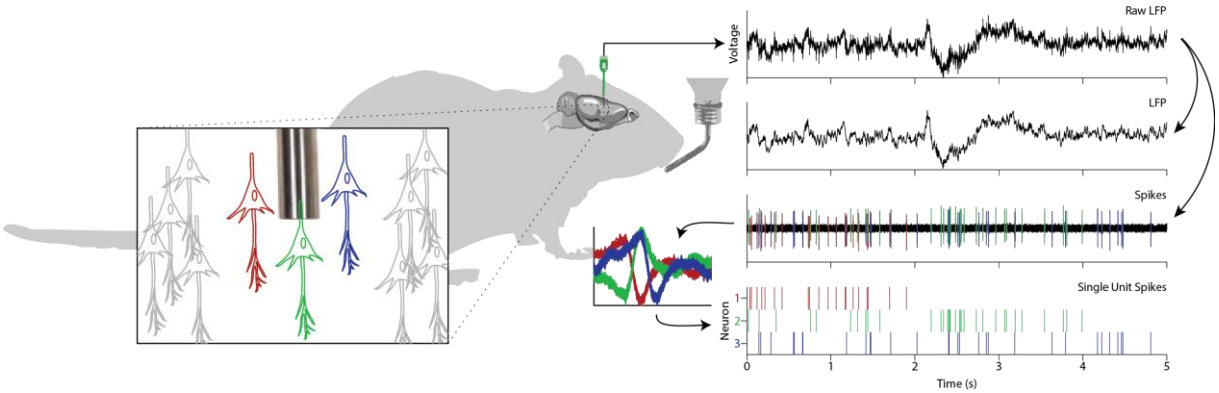

Figure 3.3 – General scheme of acquisition of local field potentials and spike times. The electrode raw signal is low-pass and high-pass filtered to separate local field potentials from spiking activity, respectively. Only spikes crossing a certain threshold were considered. Whenever possible, waveforms were used to separate single unit from multi-unit activity. Illustration kindly provided by Rodrigo Pavão.

3.2 Data analysis

All the analyses were done using Matlab® (Signal Processing and Statistical toolboxes). Filtering was done using a finite impulse response filter implemented by the *eegfilt* function of EEGLAB (Delorme and Makeig 2004), which corrects phase distortions by filtering backward and forward. The Hilbert transform was used to calculate the instantaneous phase and amplitude envelope of the signals. To estimate the power spectrum density (PSD), Welch's method was used.

Theta was defined in the 5-12 Hz range. As the LFPs within a shank were very similar (Figure 3.4), only the electrode with highest normalized theta power was used (power in theta/total power). High and low gamma were defined as the 30-60 Hz and 60-100 Hz ranges, respectively. The analyses of circular variables (such as phase) were done using CircStat Toolbox (Berens, 2009).

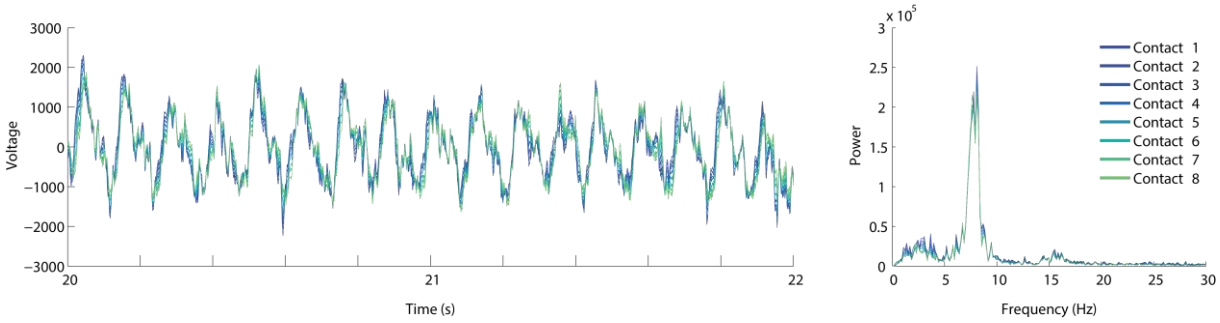

Figure 3.4 – LFP traces and PSDs in a same shank. Note all the contacts have a similar LFP profile.

3.2.1 Tracking the animal's position

The (x,y) coordinates extracted from the video files were first linear interpolated to estimate missing values generated by tracking errors. As the linear maze was not in the same axis of the camera (i.e., both coordinates had large variations), we corrected the coordinates to get most of the variance in only the x axis. To do this we calculated the velocity vectors V and used the points with high velocity (|V| > 1*standard deviation above the mean) to fit a line. As the animal was in high speed, these velocity points are supposed to be aligned with the maze axis. The coordinates were then transformed using a rotation matrix with the angle estimated by the fit. After correction, we used the x axis as the linear position of the animal in the track. Due to small differences in the distance between the camera and the maze across the sessions, we rescaled the position to vary from 0 to 250, which is the size of the maze in cm.

Because place cells in the linear track tend to be sensitive to direction the spikes on each run direction were considered independent. We separated right from left runs using the average velocity direction in a one-second window. Whenever the right and left runs showed place fields (see section 3.2.3 for the place field definition) with more than 50% of overlap, the place fields were joined as one bidirectional place field and the runs were considered together. **Error! Reference source not found.** hows the spikes of a place cell and position of the animal over time in an example session.

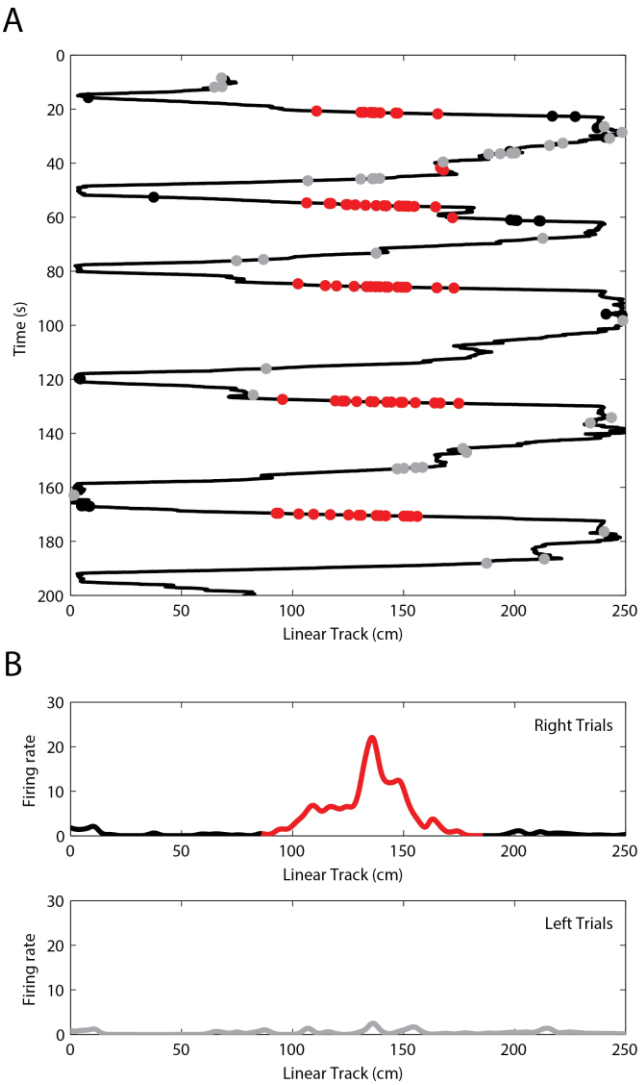

Figure 3.5 – Example of behavior and place cell activity in the analyzed dataset. (A) The animal consistently goes from one side to the other of the linear track. Each dot marks the position and time of a spike from a selected unit. Spikes in the left runs (gray dots) were separated from spikes in the right runs (red and black dots). (B) Firing rate in the right (top) and left (bottom) runs across the linear track for the entire session. The increased firing rate in red (referent to the red spikes in A) shows that this place cell mostly fires on the right trials.

3.2.2 Finding place cells

By definition, a place cell must have a higher firing rate in its place field compared to other locations. Measuring the information given by the firing rates on the animal's position can be a good parameter to estimate which cells are good candidates to be place cells. To that end, we binned the maze in 5-cm bins, and

calculated the spatial information per spike as described in the equation below (Skaggs et al., 1993):

$$I = \sum_i^N p_i \frac{\lambda_i}{\lambda} \log_2 \frac{\lambda_i}{\lambda} ,$$

where N is the number of spatial bins, λ_i is the firing rate of bin i, p_i is the probability of the animal being in bin i, and λ is the cell firing rate for the entire session. As already mentioned, the left and right runs were considered independent, thus yielding two spatial information values per cell. Figure 3.6 shows the spatial information and firing rate distribution for all cells in the dataset. We first selected as putative place cells the units with more than 1 bit of information per spike.

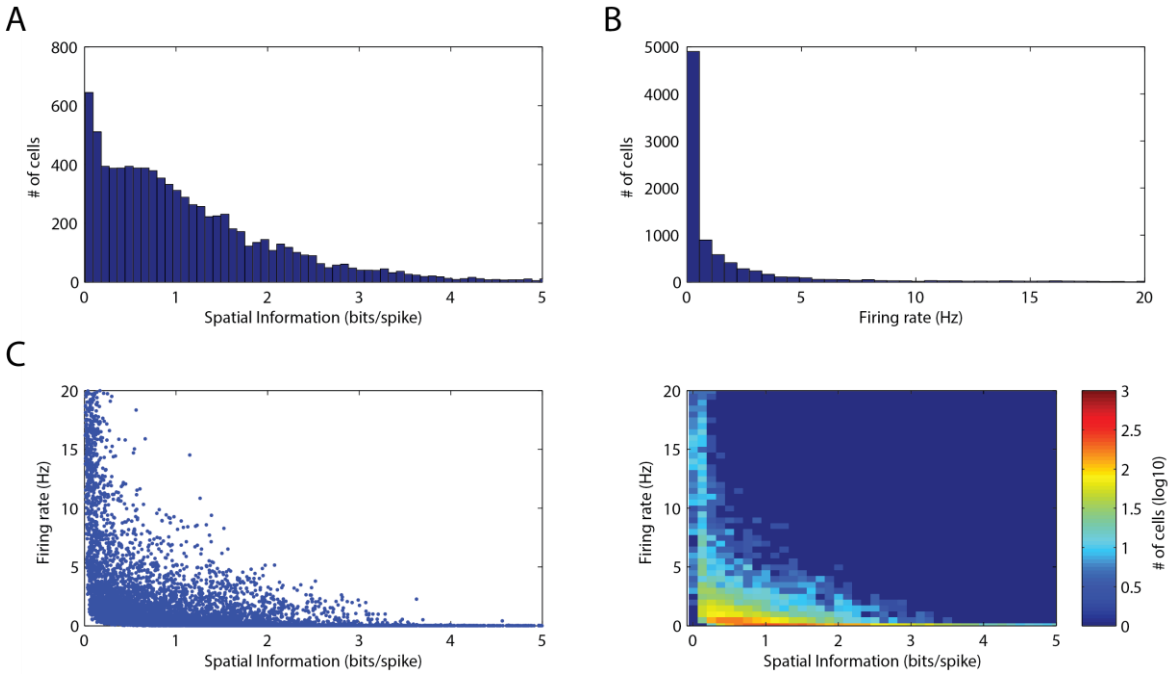

Figure 3.6 – Exploration of features of CA1 cells. (A) Distribution of spatial information (see Skaggs et al. 1996) and (B) firing rate among units. (C) Plot (left) and histogram (right) of firing rate versus spatial information for each cell.

In Figure 3.7 we show some examples of firing rates over the linear track, as well as the spatial information and firing rates for all cells. Notice that low firing rates can induce a biased measure of spatial information. To exclude cases of spurious high information, we limited our analysis to cells with firing rates higher than 0.3 Hz.

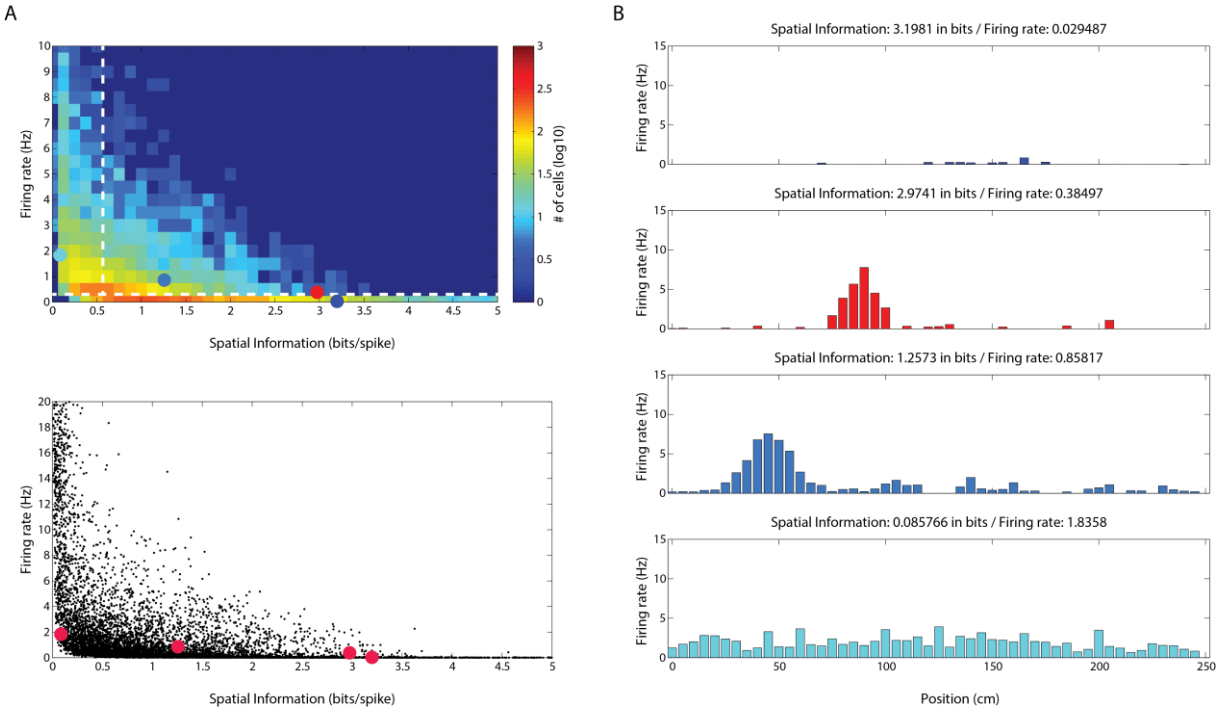

Figure 3.7 – Selection of place cell candidates. (A) Firing rate versus spatial information plot (bottom) and histogram (top). Dots (colored on top and magenta on bottom) are the cells in (B). (B) Firing rate along the track for example cells with different combinations of firing rate and spatial information. Note that high information values can arise from low firing rate (top cell).

3.2.3 Defining place fields

Once we had a pool of good candidates for place cells, we recalculated the firing rate over the track in a continuous way instead of using 5 cm bins. We convolved the spike locations (each spike was considered as an impulse) with a Gaussian kernel (5 cm of standard deviation, unitary energy) to get a continuous firing rate measure through space. This operation is described in the following equation:

$$spike\ count(x) = \int_{-\infty}^{\infty} spk(x') \cdot k(x - x')\, dx' \ ,$$

where

$$k(x) = exp\left(\frac{x^2}{2c^2}\right) ,$$

and

$$spk(x) = \sum_{i=1}^{N} \delta(x - x_i) \ ,$$

with c = 5 (the standard deviation of the Gaussian kernel), δ being Dirac's Delta function. x_i is the position of the i-th spike. In other words, this was equivalent to add, for each spike, a Gaussian function centered in the position of the animal at the spike time. This continuous firing rate was then divided by a continuous measure of the spatial occupancy calculated in the same way, that is, convolving the animal position with the same Gaussian kernel:

$$occupancy(x) = \int_{-\infty}^{\infty} position(x') \cdot k(x - x') \cdot \Delta t \cdot dx',$$

where

$$position(x) = \sum_{j=1}^{M} \delta(x - \tau_j),$$

τ_j is the position of the animal on the track at time j, M is the number of time points in which the position was sampled, and Δt is the time elapsed between two position samples. Thus, the continuous version of the firing rate over the track was defined as:

$$firing\ rate(x) = \frac{spike\ count(x)}{occupancy(x)}.$$

We considered a place field all continuous spatial intervals larger than 20 cm in which the continuous firing rate crossed a threshold. To obtain the threshold value, we first averaged all firing rate values above the median. The threshold was then defined as half of this average (a measure adapted from Senior et al., 2008). In some analyses, we extended the place field boundaries by scaling the length of the normal place field by a factor of 1.5 (which is the same of adding 25% of the normal place field to each side). Unless noted otherwise, the normal place field was used.

3.2.4 Measuring theta modulation of spikes

For each spike of each cell, we constructed a unitary vector using the LFP theta phase as the angle. After averaging all unitary vectors, the length and vector angle represented, respectively, the modulation strength and the mean phase of firing. The mean phase-vector length (MPVL) varied from 0, no modulation, to 1, maximal modulation, and the mean phase vector angle (MPVA) from 0 to 2π. They were defined by the following equations:

$$\overrightarrow{MPV} = \frac{1}{N} \sum_{j=1}^{N} e^{i \cdot \theta_j},$$

$$MPVL = \left|\overrightarrow{MPV}\right|,$$

$$MPVA = \tanh^{-1} \frac{Re\{\overrightarrow{MPV}\}}{Im\{\overrightarrow{MPV}\}},$$

where θ_j is the theta phase of the *j*-th spike and N the total number of spikes.

The spike phases were binned into 18 equally spaced phase bins to calculate the spike phase distribution (see Figure 4.2). Additionally, the preferred phase of a unit was defined as the maximal value of the spike phase distribution (notice that the preferred angle may not necessarily be the same as the mean angle in case of asymmetric spike-phase distributions). From now on we refer to MPVL and MPVA as '(theta) modulation strength' and 'mean firing phase', respectively.

3.2.5 Calculating phase precession maps

For every spike that occurred when the animal was inside the place field, we plotted the animal's position versus the theta phase. This yielded, in most cases, a banana-shaped cloud of points that is characteristic of phase precession. In some of the analyses, we binned the space and phase in 10 and 18 equally spaced bins, respectively, and calculated 2-D histograms of spike counts. To calculate a smoothed version, we convolved a high-resolution 2-D histogram (100 bins of space and 180 bins of phase) with a 2-D Gaussian, as shown in Figure 3.8. This was used to calculate the mean phase precession map.

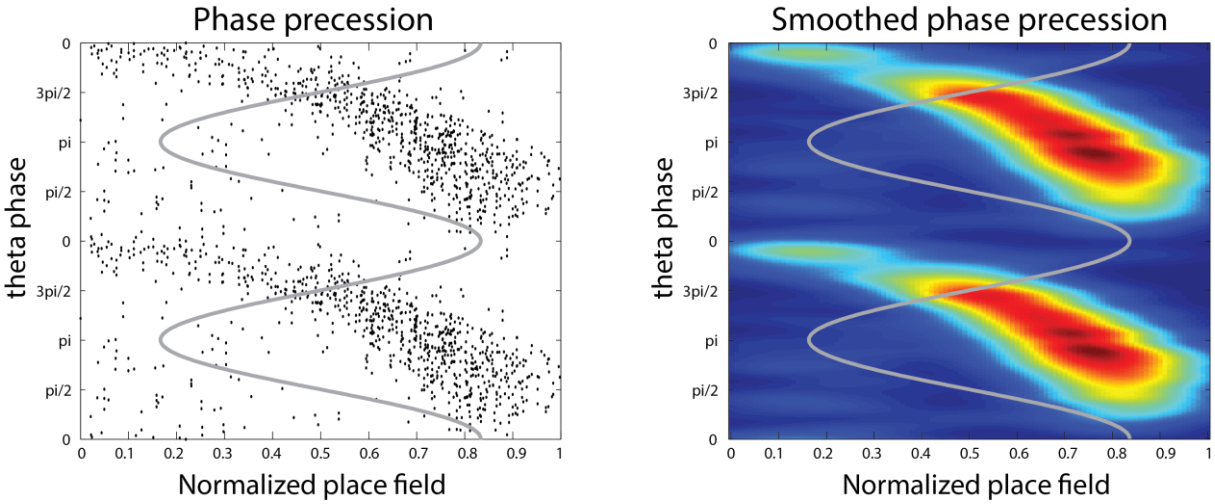

Figure 3.8 – Example of phase precession. (Left) Theta phase versus position for each spike of a place cell. The position was normalized to be 0 at the start of the place field and 1 at the end. (Right) Color coded histogram of the points in the left panel smoothed with a 2-D Gaussian.

To compare place fields of different sizes, we rescaled them to a unitary length (the positions were set to vary from 0 to 1). Because we separated left from right runs, we reflected all phase precession maps from left runs, so that 0 was always the beginning of the place field, and 1, the end.

3.2.6 Calculating the instantaneous firing rate

The instantaneous firing rate (IFR) for each spike time was calculated similarly to previous work (Harris et al., 2002;). For each spike time we counted the total number of spikes occurring one theta cycle before until one theta cycle after (Figure 3.8). Because this window was based on the theta phase, it had a variable size depending on the instantaneous theta frequency (which was estimated from the instantaneous phase). Thus, we could associate the instantaneous firing rate of a spike with its theta spiking phase and position inside the place field.

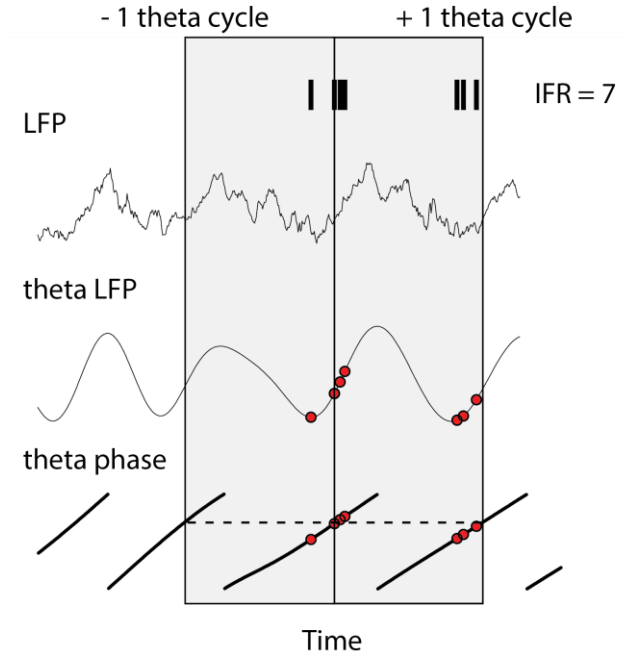

Figure 3.9 – Calculating the instantaneous firing rate (IFR). For each spike time the theta phase was accessed through the Hilbert transform of the theta-filtered LFP. The window to calculate the IFR was from the previous cycle of theta to the next one, defined by the spike phase.

3.2.7 Calculating IFR-position spiking phase maps

To explore the relation of phase, IFR, and position together, we first normalized the IFRs inside each place field to vary from 0 to 1. Then we binned the positions and the IFRs in 10 equally-spaced bins and average the theta spiking phase on each IFR-position bin. We calculated a pooled IFR-position spiking phase map (pooling together all the spikes) and a mean IFR-position spiking phase map (averaging the maps of each place cell). The maps were then smoothed with a 2-D Gaussian (because of the circular nature of phase, the smoothing was done by convolving the Gaussian with the angle vectors in Cartesian coordinates and then transformed back to polar coordinates).

3.2.8 Comparing spiking and LFP theta frequency

To compare the spike theta frequency with the LFP theta frequency we separated the spikes of every place cell in two categories: spikes that occurred when the animal was inside the place field (inside spikes), and spikes that occurred when

the animal was outside the place field (outside spikes). For each category we calculated the auto-correlogram, normalized to be 1 at the zero lag. For accessing the theta frequency of the spikes, we calculated their power spectrum density and looked for the peak value between 5 and 12 Hz. The same was done to access the LFP theta frequency. The extended place field was used in these analyses.

3.2.9 Comparing the spiking phase inside and outside the place field

To compare the spiking phase of place cells inside and outside the place field we first selected periods of high theta using the median of the theta/delta envelope as threshold. The inside and outside spikes occurring in these periods were used to calculate two spiking phase distributions, with the phases binned from 0 to 360º in 20º bins. The theta modulation strength, the mean spiking phase and average probability of firing in each phase was then calculated for the two categories.

3.2.10 Calculating the relation between spiking phase and distance to the place field center

We investigated the spiking phase depending on the distance to the center of the place field. The center was defined as the position of maximal firing rate, and the distance from the center to each spike was normalized by the length of the place field. In the case of more than one place field in the same cell, the smallest relative distance was considered. We binned the relative distance from -3 to 3 using bins of 0.1 (a symmetrical place field should be from -0.5 to 0.5, with 0 as the center) and the spiking phase in 18 equally-spaced bins. Then we calculated 2-D histograms of spike counts using these distance and phase bins, yielding the phase distance map.

3.2.11 Phase precession maps based on gamma amplitude

Phase precession maps based on gamma amplitude were obtained as theta phase precession maps calculated taking into account only the spikes that occurred in low or high amplitude of gamma. We first calculated the amplitude envelopes for the specific gamma band (LG: 30-60 Hz or HG: 60-100 Hz) in CA1 or EC layer III (EC3). We then selected the 25% higher amplitude values as the high amplitude

periods, and the 25% lower ones as the low amplitude periods (which form the fourth and first quartiles, respectively). At last, all spikes that occurred in each period were used to calculate two phase precession maps, as described in section 3.2.5.

3.2.12 Gamma amplitude variations across the place field

To see the pattern of gamma amplitude along the place field we calculated the amplitude envelope of gamma for each spike inside the place field and associated it with the spike theta phase. After binning the phase and position in respectively 18 and 10 equally-spaced bins, we averaged the gamma envelope in each bin. Thus, this graph shows the mean gamma amplitude for spikes in different theta phases along the place field.

3.2.13 Spike and LFP phase-energy plots

In this analysis, we calculated the amplitude distribution of frequencies from 20 to 200 Hz (in steps of 2 Hz) for different theta phases. For each of these frequencies we first obtained the instantaneous amplitude using the continuous Morlet wavelet and Hilbert transforms. Then theta phases were binned in 5º bins and the amplitude envelope for each frequency was averaged for each bin. The LFP phase-energy plot is obtained by a bidimensional display of the mean amplitude as function of the amplitude frequency (y axis) and theta phase (x axis).

Spike phase-energy plots were obtained in a similar way, except that only the timestamps associated with spikes were taken into account. In other words, we calculated the amplitude and phase envelopes for the whole time series but just used the data points coincident with spike times (inside or outside spike times). Additionally, the LFP was z-scored before the calculation of the amplitude envelope, so that we could pool the envelope points of different sessions/animals.

3.2.14 Quantification of phase-amplitude modulation

To see whether theta phase modulated the amplitude of any frequencies in the 20-200 Hz range, we used a modulation index (MI) described elsewhere (Tort et al., 2010). Shortly, it is the Kullback-Leibler distance of the mean amplitude

distribution (along the phases) from the uniform distribution normalized to be in the 0-1 range. The MI is described by the following equation:

$$MI = 1 + \frac{1}{\log N} \sum_{j=1}^{N} P(j) \log P(j)$$

where *N* is the total number of phase bins, and *P(j)* is the mean amplitude in the *j*-th bin divided by the sum of amplitudes in every bin.

The mean amplitudes from the phase-energy plots were averaged across place cells and the MI was calculated. To access the significance of the modulation we used a 1000 surrogate analysis. For each surrogate, the spiking phase distribution of each place cell was randomly scrambled before the calculation of the MI. A 1% confidence level was used as threshold.

4 Results

4 Results

4.1 General characteristics of place cells

Before performing novel analyses, we deemed important to first ensure that we were able to replicate classical results about place cell activity. This was indeed the case. Below we detail the main findings.

4.1.1 Place cells in the linear track

We analyzed 2921 CA1 cells and detected 599 place cells and 858 place fields distributed across three rats, as shown in Figure 4.1. The great majority of place cells had only one place field and were unidirectional (Figure 4.1A), which means they only had place fields in one direction (see **Error! Reference source not ound.** for an example of a typical unidirectional place cell).

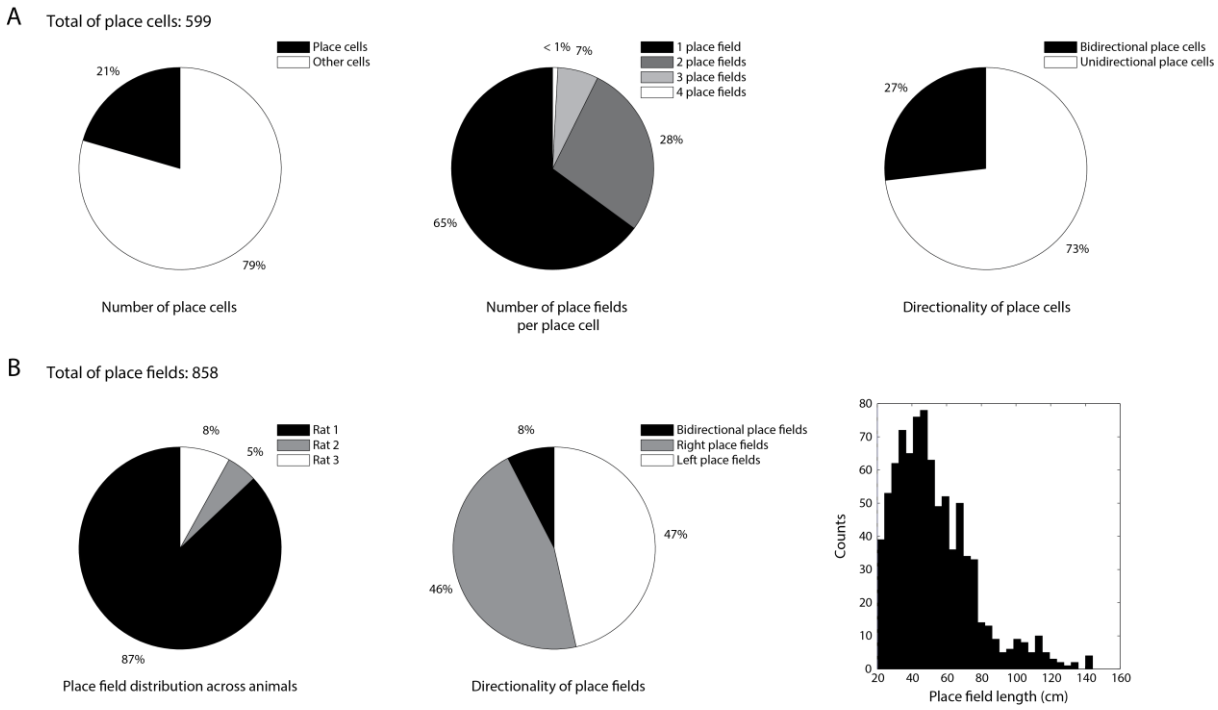

Figure 4.1 – Descriptive statistics of units in the dataset. (A) Shown are the proportion of place cells among all recorded CA1 cells (left), distribution of the number of place fields per place cell (middle), and distribution of directionality of place cells (right). (B) Proportion of place fields across animals (left), distribution of directionality of place fields (middle), and distribution of place field lengths (right).

Similarly, we also found that most of the place fields were unidirectional (Figure 4.1B middle); only ~5% of the fields were bidirectional, which were cases in which a place cell had two place fields, one in each direction, with a space overlap between fields of more than 50%. The distribution of place field lengths had a mean length of 40 cm (range: 20-144 cm; Figure 4.1B right). These findings are consistent to what has been previously described in the literature (McNaughton et al., 1983; Muller et al., 1994).

4.1.2 CA1 cells and theta oscillations

Pyramidal cells, and place cells in particular, tend to fire at the valley of the theta oscillation recorded from the pyramidal cell layer. The negative voltage in the LFP indicates that positive currents are entering the cells, thus yielding a higher firing probability. In our analyses, the mean firing probability across all CA1 cells peaked at the pyramidal theta valley (Figure 4.2A). Looking separately to each cell, we confirmed that most of them had the preferred phase and the mean firing phase (see section 3.2.4 in Methods) at the theta valley (Figure 4.2B,D). The modulation strength varied from 0 to 0.4, peaking around 0.1 (Figure 4.2C).

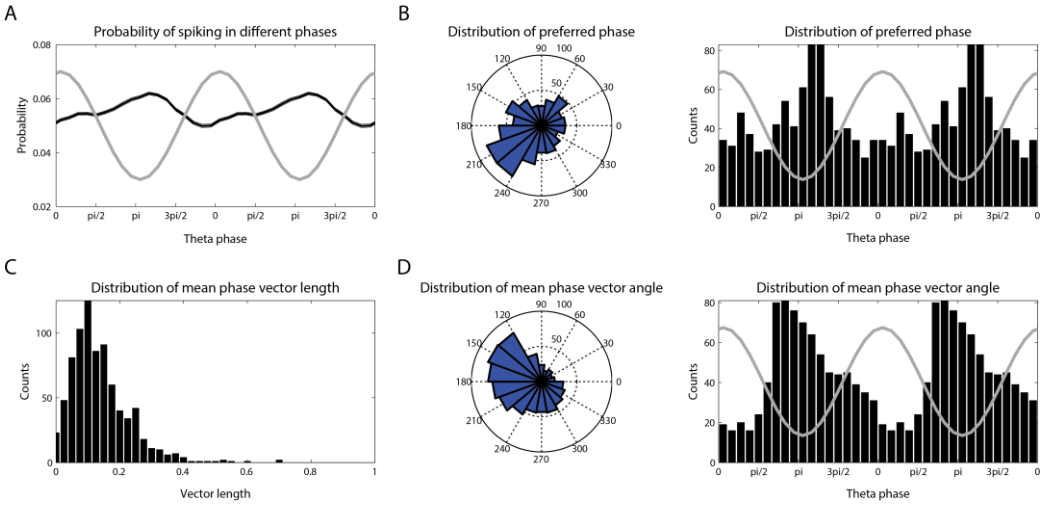

Figure 4.2 – Modulation of CA1 spiking activity by the hippocampal theta rhythm. (A) Mean (μ ± SEM) spiking probability at each theta phase. (B) Preferred phase and (D) mean spiking phase histogram for all units. (C) Distribution of mean phase vector length. Reference theta cycles are shown in the gray lines.

4.1.3 Place cells, theta oscillations and phase precession

We next restricted the analyses above to place cell spikes occurring inside the place field (Figure 4.3). We found that the modulation strength was a little bit higher, peaking at 0.2 (Figure 4.3A), while the preferred phase and mean spiking phase distributions were similar (Figure 4.3B). As described by Recce and O'Keefe (1993), the phase of theta in which spikes occurred varied as the animal crossed the place field. The theta phase-position 2-D histogram of spike counts showed that at the beginning of the place field the spikes occurred most at the ascending phase of theta, close to the peak (see Figure 4.3D). In the center of the place field, the number of spikes increased, and the phase of most spikes was the theta valley. At the end of the place field the firing rate decreased and the spikes occurred at the descending phase of theta (although spikes were less phase specific at this point).

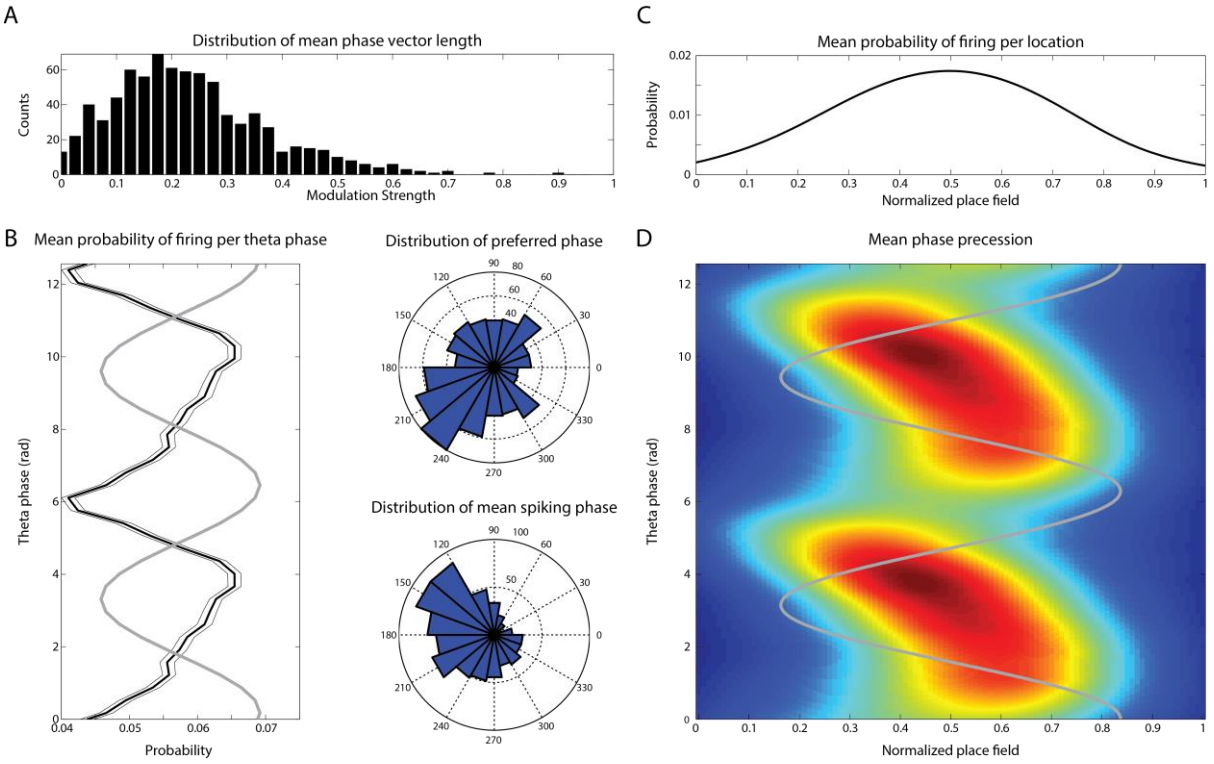

Figure 4.3 – Modulation of place cell spiking activity by the hippocampal theta rhythm. (A) Histogram of the modulation strength of all place cells. (B) Mean probability of spikes in different phases of theta (μ ± SEM) (left) and distribution of preferred phase and mean spiking phase inside the place fields (right). (C) Mean probability of firing along the place field. (D) Mean phase precession plot for all place cells. Reference theta cycles are shown in the gray lines.

4.2 Relation between spatial information, firing rate and theta modulation of place cells

Place cells have spatial correlates of firing rate which yield information about the animal position. Because of the intrinsic relationship between place cell firing and the theta rhythm (the phase precession), we investigated the dependency of these variables and the theta modulation of spikes. To do so, we first calculated the spatial information and total firing rate for each place cell and looked for a relation between them and the mean spiking phase (Figure 4.4). We found no difference in the mean spiking phase across cells with different firing rates (Figure 4.4A) and different spatial information content (Figure 4.4B), suggesting that these variables are independent.

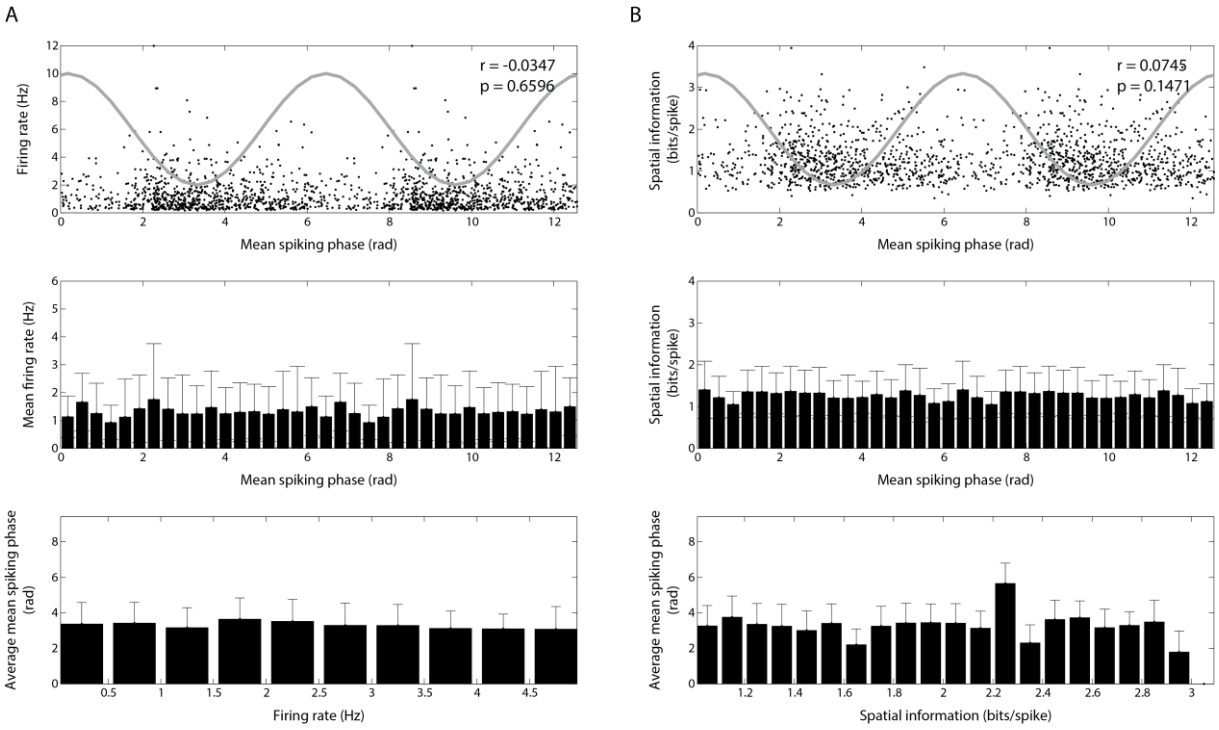

Figure 4.4 – Mean theta phase of spiking vs. firing rate and spatial information. (A) Dispersion plot of mean spiking phase and firing rate (top), mean firing rate over each mean spiking phase bin (middle), and average mean spiking phase for different firing rate bins (bottom). (B) Similar to (A) but using spatial information instead of firing rate. Notice that there is no apparent dependency of neither firing rate nor spatial information on mean spiking phase. Error bars represent the standard deviation. The last bar includes all points beyond the last bin. Circular-linear correlation coefficients and associated p-values are shown in the top panels.

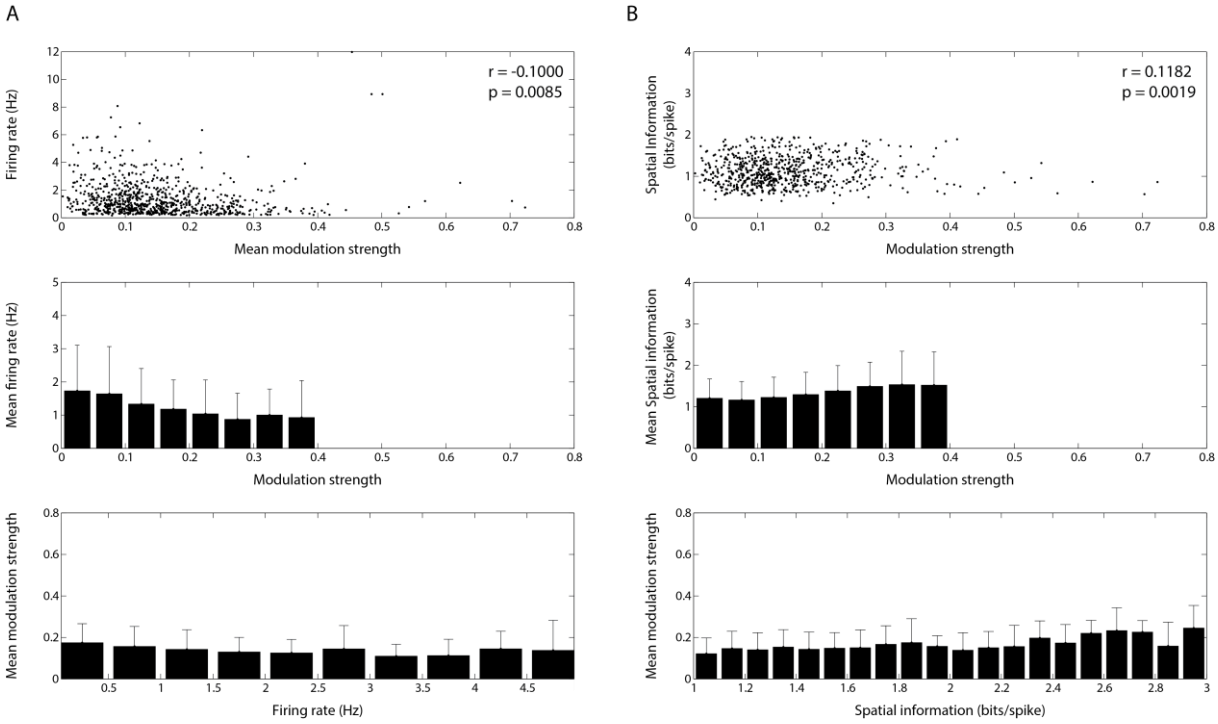

Figure 4.5 – Modulation strength vs. firing rate and spatial information. (A) Dispersion plot of modulation strength and firing rate (top), mean firing rate for different modulation strengths (middle), and mean modulation strength for different firing rates (bottom). (B) Similar to (A) but using spatial information instead of firing rate. Notice a small but significant negative correlation between firing rate and modulation strength, as well as a small significant positive correlation between spatial information and modulation strength. Error bars represent the standard deviation. The last bar includes all points beyond the last bin. Linear correlation (Pearson) coefficients and associated p-values are shown in the top panels.

Similarly, we compared the firing rates and spatial information with the strength of theta modulation of spiking activity (Figure 4.5). We found a small correlation for the firing rate to decrease with theta modulation strength (Figure 4.5A), and a small correlation for the spatial information to increase with modulation strength (Figure 4.5B).

4.3 Spiking phase dependency on position and firing rate

To investigate the nature of the phase precession phenomenon, we repeated analyses performed in Harris and colleagues (2002), Huxter and colleagues (2003), and Cei and colleagues (2014). We first calculated the theta phase, instantaneous firing rate (IFR) and relative position inside the place field for all the (inside) spikes. Then a 2-D color-coded histogram of spike counts was calculated for either (phase,

position) or (phase, IFR) pairs across the pool of all spikes from all place fields (Figure 4.6B,C top).

The histograms showed that there was little phase specificity for different values of IFR (Figure 4.6B top). This is somehow expected because similar rates occur at both the beginning and end of the field, which are associated to different spiking phases. In the case of position, the spiking phase distribution was more concentrated at the beginning of the field compared to the end (Figure 4.6C top).

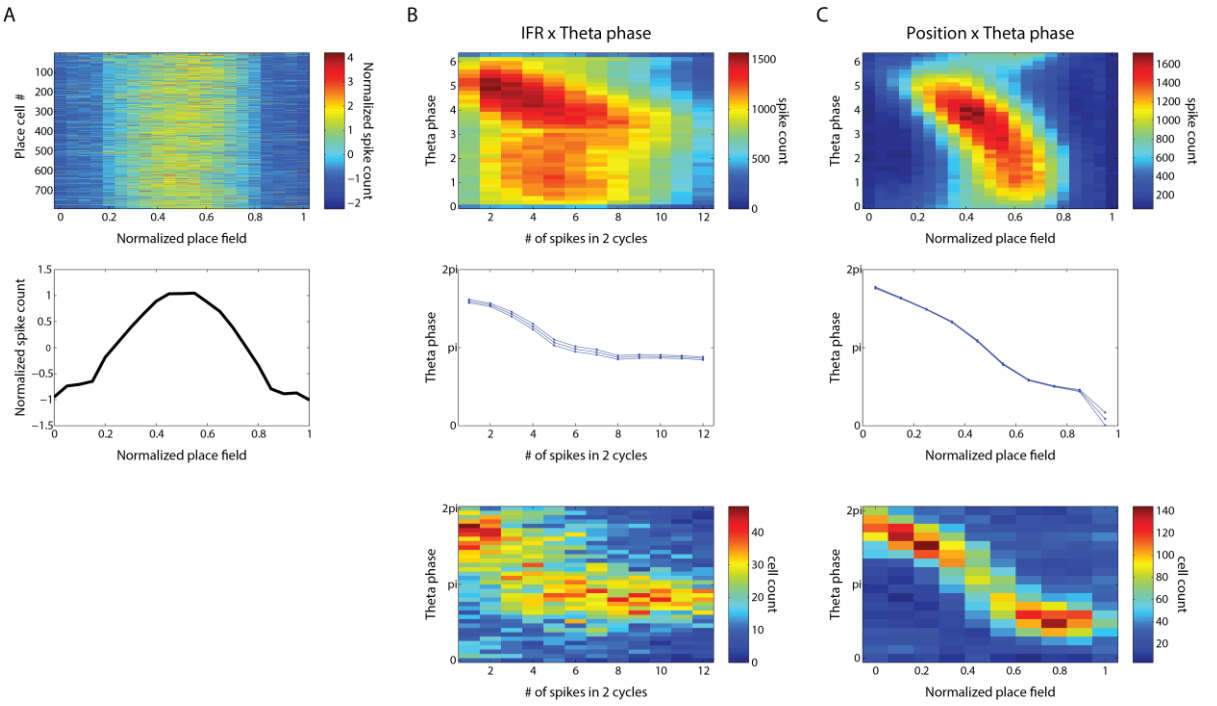

Figure 4.6 – Spiking theta phase relation with firing rate and position. (A) Normalized spike count (z-score) along the field for each place cell (top) and mean spike count (bottom). (B) Histogram of spike counts per instantaneous firing rate (IFR; see Methods) and theta phase (top). Spikes of different place cells were pooled. The circular mean phase with 95% confidence intervals are shown in the middle plot. The bottom panel shows the number of place cells per IFR and mean spiking phase. (C) Histogram of spike counts per position along the place field and theta phase (top). Spikes of different place cells were pooled. The circular mean phase with 95% confidence intervals are shown in the middle plot. The bottom panel shows the number of place cells per position and mean spiking phase.

We next calculated the average phase for all spikes for both IFR and position along the place field. This is similar to what was done in Harris and colleagues (2002) for IFR (Figure 1.7). Similar to them, we found that the mean spiking phase

decreases with IFR (Figure 4.6B middle). The same effect is present when we analyze the mean spiking phase as a function of position (Figure 4.6C middle). To check whether this result was not influenced by few place cells with abundant spikes, we calculated the mean spiking phase per IFR or position for each place cell separately. The 2-D histogram of cell counts for different mean spiking phase and IFR (Figure 4.6B bottom) or position (Figure 4.6C bottom) provided similar results as found in the pooled analyses.

Next we calculated circular correlation coefficients between spiking phase and IFR or position for each place cell as in Huxter and colleagues (2003). As in their work (Figure 1.8), the mean of significant r values ($p<0.05$) was significantly higher for position than for IFR (Figure 4.7A). A histogram of the r values confirmed that spiking phase correlates better with position than with IFR (Figure 4.7B). To analyze the mutual dependency of the three variables, we computed IFR-position spiking phase maps for the pooled spikes (Figure 4.7C left), as well as the mean map over individual cells (Figure 4.7C right). These analyses, as in Cei and colleagues (2014) (Figure 1.9), showed no horizontal or vertical stripes, which would be expected if the spiking phase were only dependent on either position or IFR. Rather than that, it seems that none of these variables alone can explain spiking phase variations.

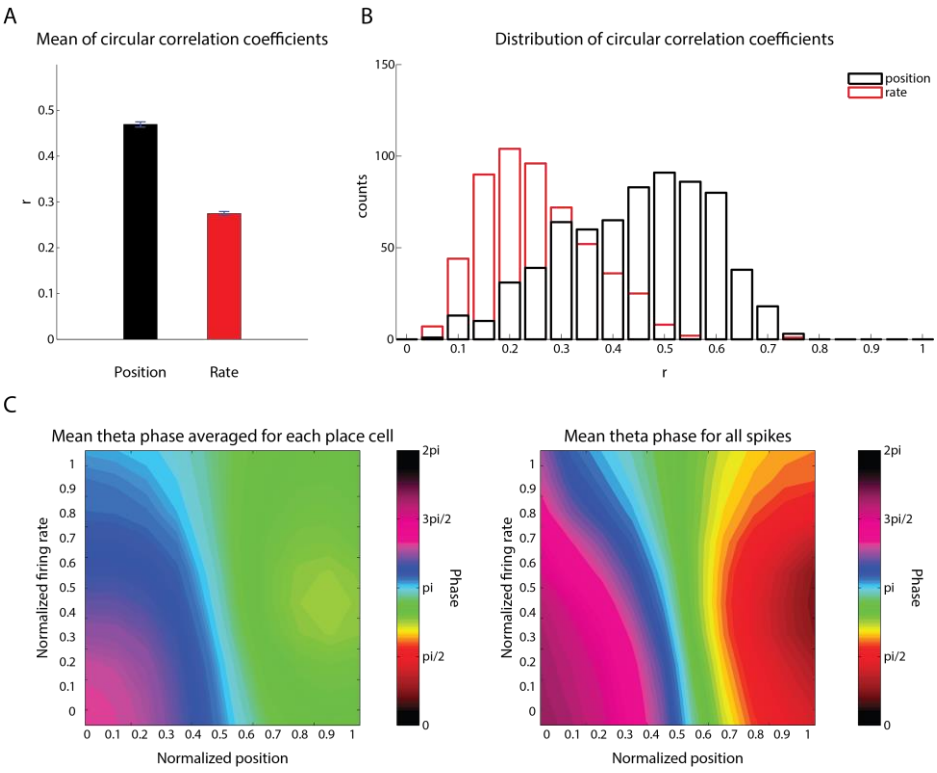

Figure 4.7 – Spiking phase dependency on firing rate and position. (A,B) Mean (A) and histogram (B) of circular correlation coefficients for spiking phase and position and spiking phase and IFR. (C) Mean theta phase in each (position, rate) pair for pooled spikes (left) and individual place cells (right).

4.4 Differences in place cell activity inside and outside the place field

For each place cell, we accessed the theta frequency of spikes inside and outside the place field and compared with the CA1 LFP theta frequency. Figure 4.8 shows the mean auto-correlogram for spikes and CA1 LFPs (Figure 4.8A,D), as well as the mean PSD (Figure 4.8B,E). The auto-correlograms revealed peaks corresponding to the period of theta oscillations for both inside spikes and LFPs (Figure 4.8A,D), which was reflected in the PSD by a power peak in the theta range (Figure 4.8B,E). The PSD also revealed a theta power peak for the outside spikes, even though this theta activity was not very apparent in the auto-correlogram for these spikes. Finally, the histograms of theta peak frequencies (Figure 4.8C,F), showed that the theta frequency of inside spikes was higher than the LFP theta peak frequencies. Regarding the outside spikes, however, the theta peak frequencies were more distributed, across 5 to 10 Hz.

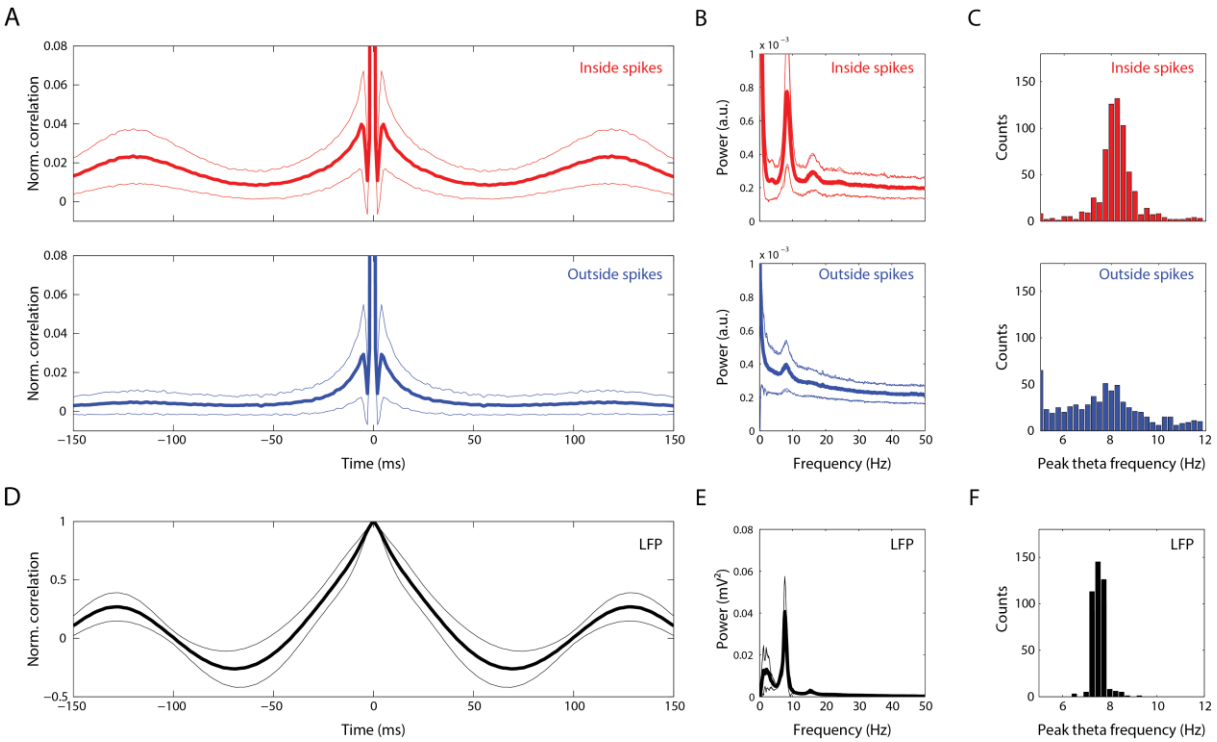

Figure 4.8 – Theta frequency of spikes and LFPs. (A,D) Mean auto-correlogram of inside (top; red) and outside (bottom; blue) spikes (A) and LFPs (D). (B,E) Mean PSD of inside (top; red) and outside (bottom; blue) spikes (B) and LFPs (E). (C) and (F) show the peak frequency histogram for inside and outside spikes and LFPs, respectively. Thin lines represent μ ± SD.

We next explored potential differences between inside and outside spikes in relation to their theta firing phase. Figure 4.9A shows that inside spikes have higher probability of occuring at the theta valley than outside spikes. This was confirmed by the mean spiking phase histograms (Figure 4.9B right), which show high counts in opposite phases, although their modulation strength had similar distributions (Figure 4.9B left).

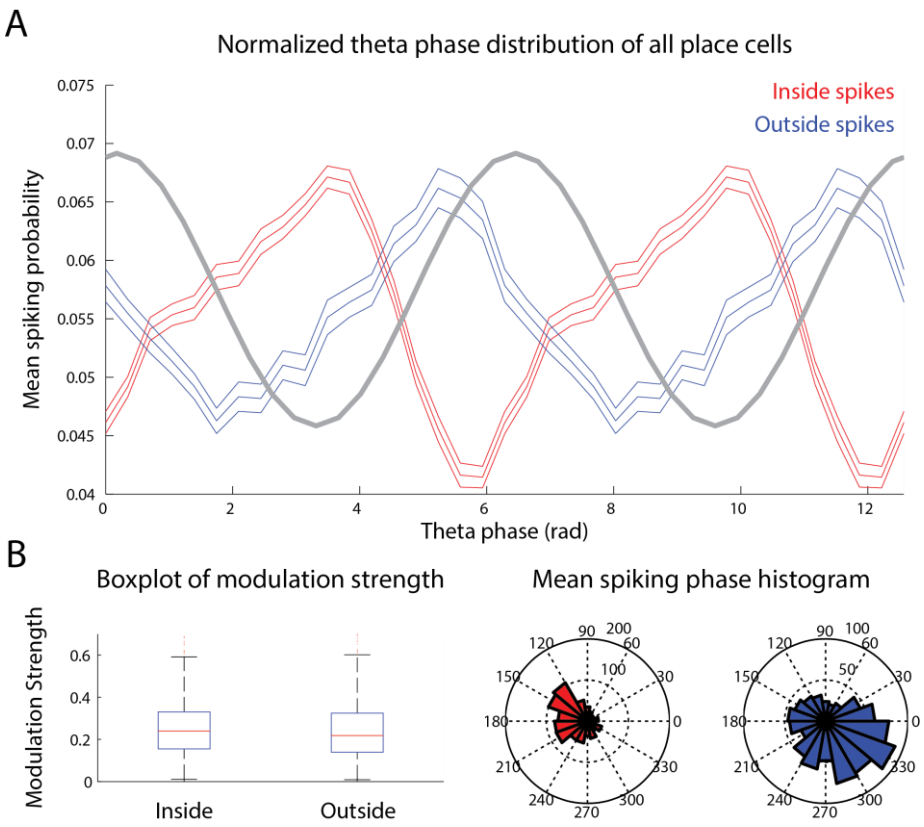

Figure 4.9 – Mean spiking phase inside and outside the place field. (A) Mean spiking probability for different theta phases for inside (red) and outside (blue) spikes (μ ± SEM). (B) Boxplot of modulation strength (left) and mean spiking phase histogram for inside and outside spikes. The two distributions have different means (Watson William test; $p<0.001$)

Since our definition of the place field boundary was operational, and rather arbitrary, and could thus be narrower or wider than the 'actual' place field, we repeated the analyses above using an extended definition of place field (see Methods). We found a similar theta phase distribution for the inside spikes probability. However, under this analysis protocol, the spiking phase probability for

outside spikes showed a bimodal distribution (Figure 4.10A). As the firing inside the place field is supposed to precess, and because of the discrepancy between the results obtained under different definitions of place field boundaries (see Discussion), we next investigated the spiking phase as a function of the distance to the place field center (as described in section 3.2.10). This distance was normalized in units of place field length, so that 0 corresponds to the center of the field (the position of maximal firing rate) and the interval between -0.5 and +0.5 corresponds to the original place field length. We found that the phase precession started far before -0.5, that is before the original place field boundary (Figure 4.11B,C). Spikes occurring 1 place field from the center already preferred the ascending phase of theta, even though at this position the firing rate increase was very slight (Figure 4.11C,D). Outside spikes occurring before -2.0 and after +1.5 field length exhibited phase preference for the theta valley (Figure 4.11B,C).

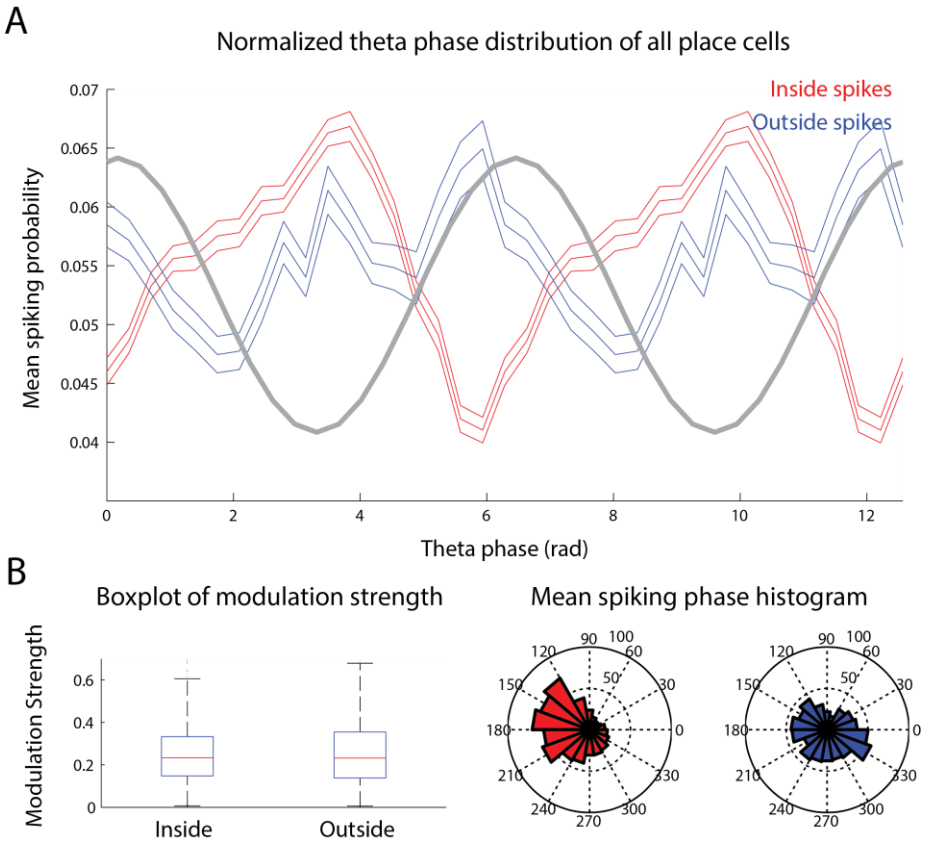

Figure 4.10 – Mean spiking phase inside and outside the place field using extended boundaries. (A) Mean spiking probability for different theta phases for inside (red) and outside (blue) spikes (μ ± SEM). (B) Boxplot of modulation strength (left) and mean spiking phase histogram for inside and outside spikes. The two distributions have different means (Watson William test; $p<0.001$).

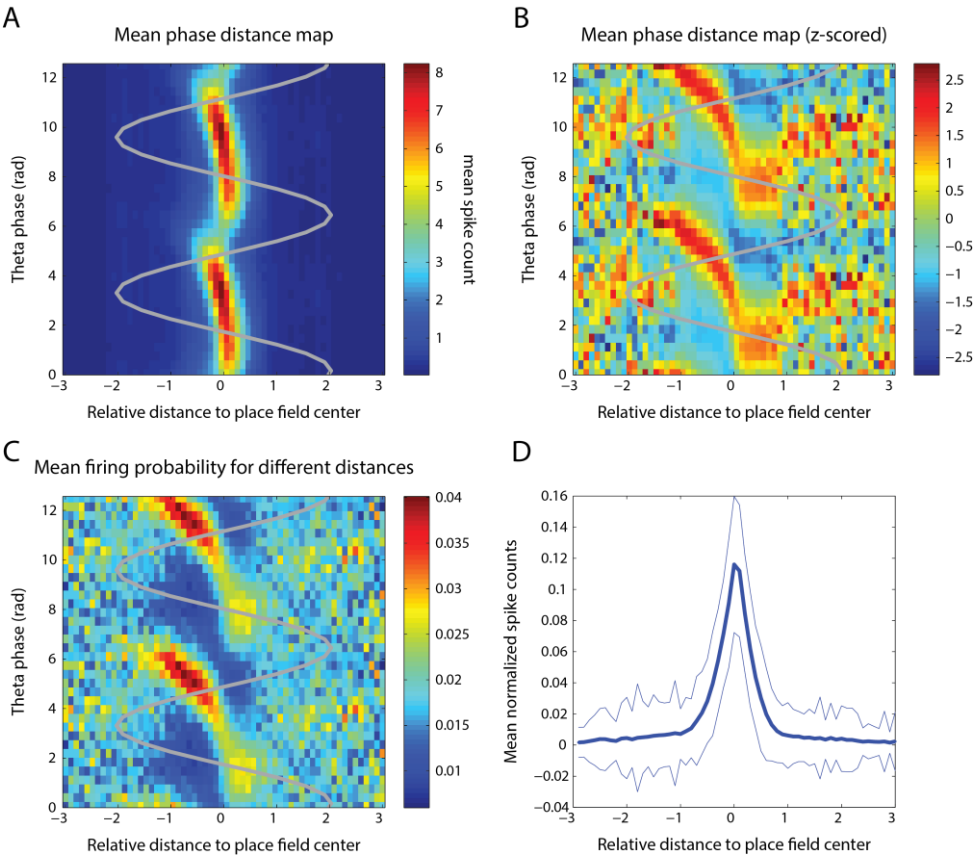

Figure 4.11 – Theta spiking phase in function of the distance to the place field center. (A) Mean phase-distance map across all place cells. The color scale represents mean spike count. (B) Same as in A but z-scored along the columns to control for the higher spike counts in the center of the field. (C) Mean firing probability over theta phases for each relative distance. (D) Mean normalized spike counts along the relative distance axis. Normalization was performed for each cell by dividing by the total number of spikes. Note that spiking phase coordination begins before 1 place field length.

4.5 Place cell spiking and low and high gamma oscillations

To explore the relation of place cells to low and high gamma activity, we first calculated phase precession maps based on gamma amplitude in LFP recordings from CA1 or EC layer III. We found that separating high and low amplitudes of HG and LG also separated spikes into different phases and positions inside the place field for both CA1 (Figure 4.12A,C) and EC3 (Figure 4.13A,C) gamma oscillations. The results were corroborated by analyzing the coupling between theta phase and gamma amplitude restricted to timestamps associated with spikes along the place field, which showed highest gamma at the descending phase of theta (Figures 4.12B,D and 4.13B,D). This was valid for both CA1 and EC3 gammas.

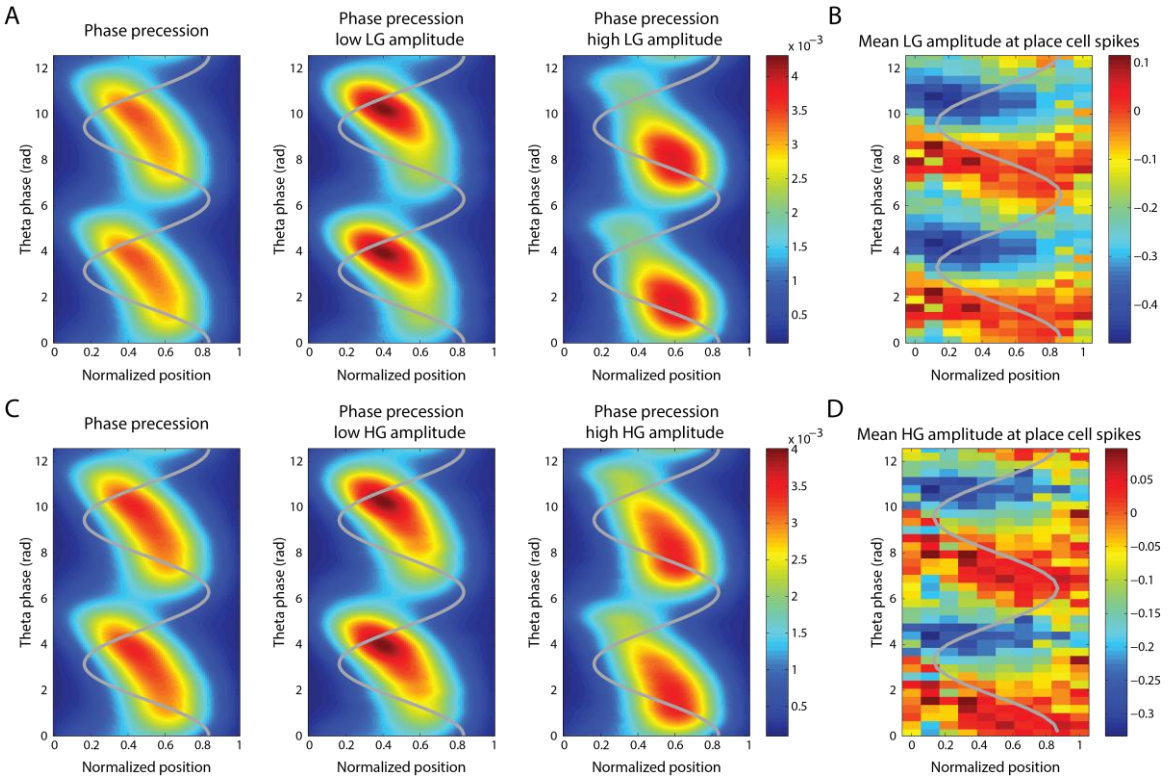

Figure 4.12 – CA1 gamma oscillations and phase precession. (A) Phase precession map for all spikes (left) and for spikes during low (middle) and high (right) amplitude of LG. (B) Mean amplitude of LG for spikes in different theta phases and positions inside the place field. (C,D) Same of (A,B), but for HG.

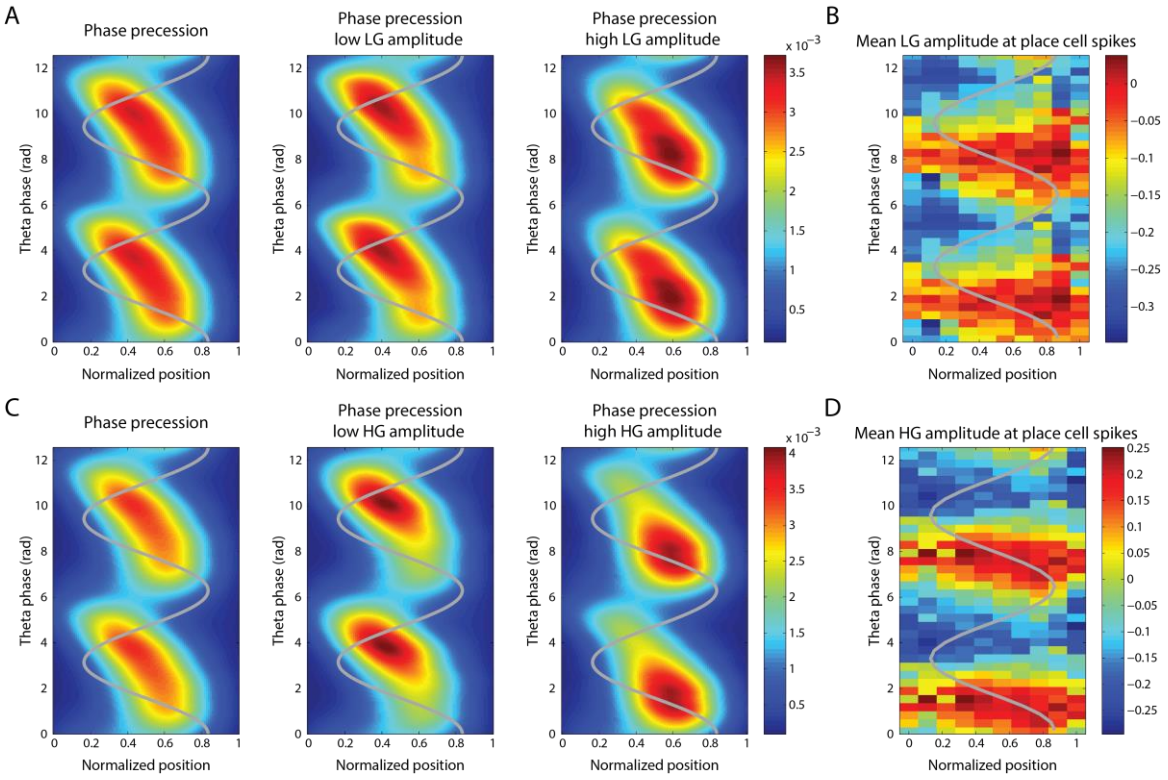

Figure 4.13 – Same as Figure 4.12, but for EC3 gamma oscillations.

Therefore, these results show that periods in which gamma amplitude is low are associated with the beginning of the phase precession; conversely, gamma amplitude is high at the end of the phase precession.

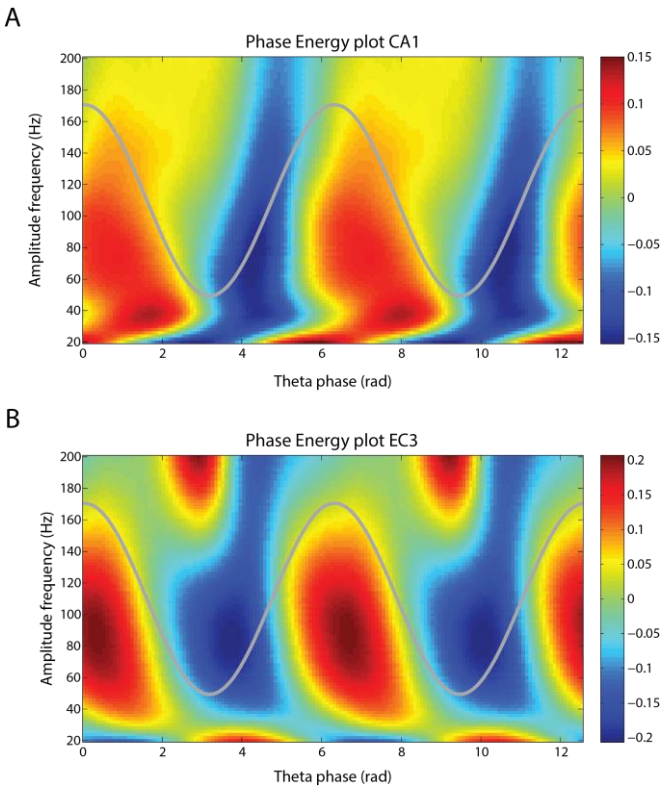

Figure 4.14 – Mean phase energy distribution of CA1 (A) and EC3 (B) LFPs for amplitude frequencies from 20 to 200 Hz. Reference theta was recorded from the CA1 pyramidal layer.

We next looked to the theta phase-energy distribution of EC3 and CA1 LFPs in frequencies from 20 to 200 Hz. In both EC3 and CA1 we found a strong modulation in the HG range (60 to 140 Hz), with maximal amplitude at the descending phase close to the theta peak (referenced to the pyramidal cell layer) (Figure 4.14). Additionally, CA1 also presented modulation in LG at the descending phase (near to the theta valley) of the pyramidal cell layer theta.

In a similar analysis, we looked to phase-energy plots of EC3 and CA1 LFPs restricted to spike times of CA1 place cells. In this analysis we separated inside from outside spikes using the extended place field definition. In CA1 LFPs, we found a significant theta phase modulation of the amplitude of 40-80 Hz band when the analysis was restricted to the inside spikes (Figure 4.15). This comodulation was absent in all other cases. Additionally, a small increase in the 20-40 Hz band was present in EC3 LFPs.

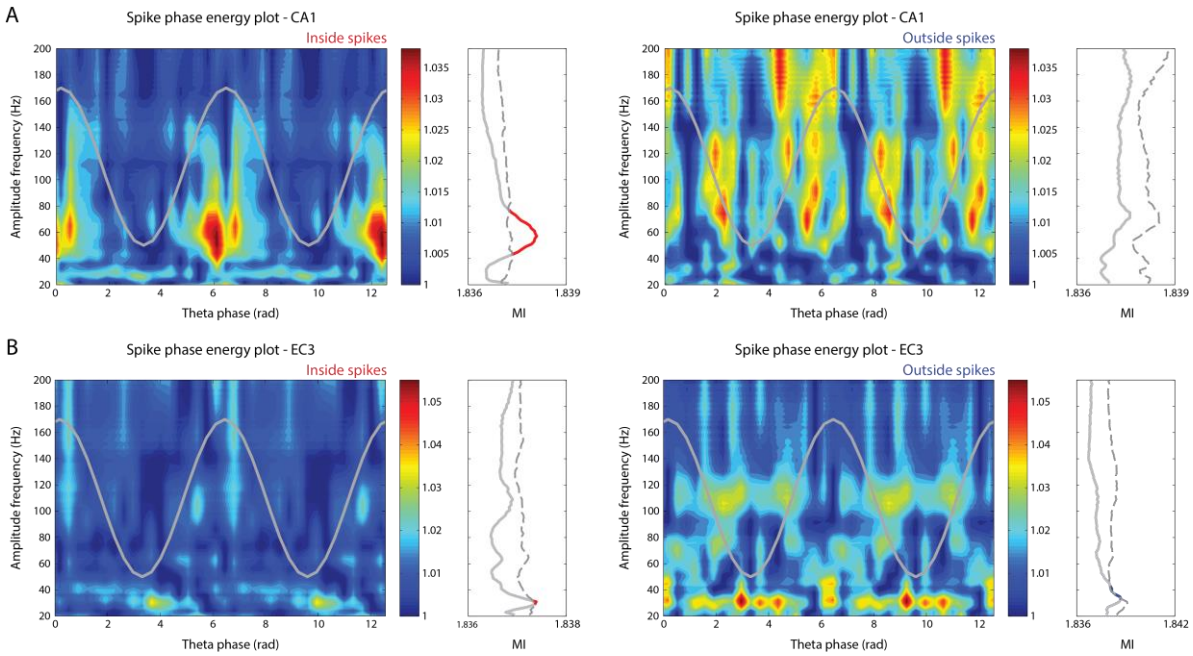

Figure 4.15 – Mean phase energy distribution for inside and outside spikes. (A) Phase energy distribution (left) and modulation index (right) calculated using LFP from CA1 for the amplitude frequencies. (B) The same as in (A), but using LFP from EC3 to extract the amplitude frequencies. Theta phase reference was obtained from CA1 for both (A) and (B). Dashed lines indicate the confidence level of the surrogate analysis ($p<0.01$).

5 Discussion

5 Discussion

The first part of the work done for the present dissertation was focused on exploring consolidated results about place cell activity in the particular dataset we used. As expected, these analyses showed very similar findings to what is classically described in the literature concerning CA1 cells. In particular, we found preferential firing of CA1 neurons at the (pyramidal) theta valley (Buzsáki et al., 1983; Fox et al., 1986), and many CA1 cells showed spatial selectivity (O'Keefe and Dostrovsky, 1971; Olton et al., 1978b). Of note, our analysis showed similar probability of firing across the phases of pyramidal theta oscillations compared to a previous work that used the same dataset (Mizuseki et al., 2009). Most of the CA1 place cells had unidirectional fields, as previously described in linear tracks (McNaughton et al., 1983; Muller et al., 1994), and their place fields could be roughly described as having a Gaussian shape (O'Keefe and Dostrovsky, 1971). We were also able to robustly reproduce the phase precession phenomenon (O'Keefe and Recce, 1993), specially on the average activity, despite having to scale place fields of different lengths.In the second part of our work, we investigated if the spatial selectivity or the firing rate of place cells were influenced by the theta modulation of spiking. Because the intrinsic relation of theta oscillations and place cells, we considered that the strength of theta-phase coupling could be a factor influencing other place cell properties. To the best of our knowledge, we are not aware of previous studies performing similar analyses, so these can be regarded as novel results. We found that the mean spiking phase had no influence on either spatial information or firing rate. On the other hand, spatial information and firing rates showed a small tendency to, respectively, increase and decrease with higher values of modulation strength.

When investigating the nature of the phase precession phenomenon, we successfully replicated three main analyses from previous works (see Figure 1.7, Figure 1.8 and Figure 1.9) and, additionally, modified them to look for consistency over place cells instead of pooled spike counts. In general, we found very similar results to the ones previously described in literature. First, both the instantaneous firing rate (IFR) and position correlated with theta phase as in Harris and colleagues (2002) (Figure 4.6; compare with Figure 1.7). Also, the correlation coefficients for phase and position were higher than for phase and IFR as in Huxter and colleagues

(2003), although the correlation coefficients for IFR and phase obtained here were higher than in this latter work (Figure 4.7; compare with Figure 1.8). This might be due to the differences in the calculation of the IFR: while we use the number of spikes in two theta cycles, Huxter and colleagues normalize the spike count by time, making their measure in Hz.

The fact that IFRs are not strongly correlated to spiking phase is explained by the Gaussian shape of firing rate along the place field, in which the spiking phases precess from ~360 degrees at the beginning of the field to ~45 degrees at the end (that is, from the peak to the descending phase of the theta wave recorded at the pyramidal cell layer). Because the spiking phase varies in a systematic way across the place field, small values of IFR are associated with two different preferred phases, namely the ones at the beginning and end of the place field. This clearly leads to a low linear correlation between these variables. Yet, there is no guarantee that the mechanisms ruling place cells activation are linear. For example, a possible rate dependent mechanism for modulation of spiking phase could work in the initial part of the place field (Figure 4.11), where the precession is more linear and evident. The subsequent firing rate decay along with no major changes of spiking phase could be due to intrinsic properties of the system returning to the steady state. Additionally, Harris and colleagues (2002) also found a similar IFR-phase relation in non-spatial behaviors such as paradoxical sleep and in a running wheel, which cannot be explained by the firing rate-position dependency.

To elucidate this problem, Cei and colleagues (2014) proposed to measure the variations of spike phase along IFR and position axes at the same time. This would overcome any dependency between these variables (which we know exists) and show a clearer picture of the spike phase dependency. Inspired by this recent work, we calculated the mean phase for pairs of (IFR, position) values. If phase depended on only one variable, we would expect vertical (for a pure position modulation) or horizontal (for a pure IFR modulation) stripes with constant spiking phase. Instead, we found diagonal stripes, indicating that phase varies with IFR for constant positions and varies with position for constant IFRs (Figure 4.7; compare with Figure 1.9). This conciliates the findings of both Harris and colleagues (2002) and Huxter and colleagues (2003).

Because most of place cell spikes occur inside the place field, spiking tendencies – if they exist – that happen outside the place field remain unnoticed in general analyses that take all spikes into consideration. Here we investigated if the spiking phase of place cells was different inside and outside the place field. We consistently found that inside the place field most spikes occurred at the theta valley. This was somehow expected since the maximal firing rate of place cells occurs in the middle of the place field and, there, phase precession plots reveal that the spikes tend to occur at theta valley. Also, the phases of spikes in the beginning and end of the place field cancel each other out (in an angular sum), resulting in a mean phase also in the theta valley.

On the other hand, at a first analysis, we found that spikes emitted outside the place field showed a tendency to occur at the ascending phase of theta (Figure 4.9). However, this was later shown to arise from limitations in our definition of the place field. Namely, when we extended the field boundaries, we found that the outside spikes occurred in a bimodal distribution that peaked in the ascending phase and at the theta valley (Figure 4.10). To eliminate any doubts about the phase of the outside spikes, we analyzed the spiking phase as a function of the distance to the field center (defined as the point with maximum firing rate; Figure 4.11). The place fields were normalized by their length and averaged. As shown in Figure 4.11, this analysis showed that phase precession started much earlier (at -1) than expected for a symmetric field (-0.5; that is, considering that 0 is the center of the field, one place field would cover from -0.5 to 0.5). The end of the place field was also underestimated, although to a lesser extent.

This analysis further revealed that the spiking probability peak at the ascending phase in Figure 4.9 was probably due to spikes occurring at the beginning of the place field, which were not included as “inside spikes” by the definition of field boundaries originally employed by us. When we extended the definition of the place field, we were able to include more spikes happening at the beginning of the field as inside spikes. Consequently, this led to lower spikes at the ascending phase as being regarded as “outside spikes”, and created a bimodal distribution for the latter (Figure 4.10). We believe the other spike probability peak at the theta valley might be the real preferred phase for the outside spikes. But because this is the same preferred phase of place cells inside the place field, at this point we cannot rule out that this finding is

not a result of spiking phase occurring in “place fields” that did not meet the criteria to be regarded as such (see Methods for the definition of place field employed here).

This analysis also showed two interesting features about place fields. First, if one considers that the place field starts and finishes at, respectively, the beginning and end of phase precession, and also considers that the center of the place field is the position of peak firing rate, then our results imply that place fields are asymmetric, skewed to the left (see Figure 4.11). In fact, place fields in the linear track are known to be symmetric in the beginning of an experience, when the rat is in a novel environment; then they gradually change to asymmetric place fields within a dozen laps (Mehta et al., 2000). Second, the results show that before the field center the spiking phase variation is much higher than after. This could indicate two different operating modes of place cells separating the future location from the past/current position of the animal, which are likely to have different behavioral importance. Furthermore, it has been shown that most of EC3 principal neurons fire at the peak of pyramidal theta, while principal neurons in CA3 fire at the descending phase of pyramidal theta (Mizuseki et al., 2009). As these phases matches the firing phases of place cells at the beginning and end of the place field, we speculate that the place cell firing at the beginning of the place field is supported by EC3 firing, conveying information of the animal’s current position, while at the end it is supported by CA3 firing, providing information of past positions. The gradual change of input weights could then explain the phase precession phenomenon.

Consistent with previous reports (Geisler et al., 2010; Mizuseki et al., 2009), spectral analysis showed that the spikes of place cells inside the place field are oscillatory and have concentration of power in the theta range (Figure 4.8A,B). Interestingly, we were able to replicate the difference in the theta peak frequency of place cell spikes compared to the theta peak frequency exhibited by LFP recordings, in which the theta of spiking activity is faster than the LFP theta. It was theorized that, because of phase precession, the spikes should oscillate in a faster theta than the LFP, as observed here. Geisler and colleagues (2010) have confirmed this hypothesis and proposed a model of phase precession generation using the interference pattern of two oscillators of slightly different frequencies (Geisler et al., 2010).

In addition to the analysis above, here we also investigated the spike theta peak frequency separately for inside and outside spikes using our extended place field. While the inside spikes showed a clear peak above 8 Hz, the outside spikes showed more distributed theta peaks (Figure 4.8C). This suggests that spikes inside the place field are better organized to have a faster theta frequency than the outside spikes, and is consistent with the existence of at least two states of spiking for place cells. We note that having no behavioral correlate to outside spikes does not mean they are not coding for other attributes. It seems that such a clear correlate of neural activity exhibited by place cells has stolen the spotlights of other functions these neurons may have, and even of the putative function of the hippocampal region as a whole, despite strong evidence pointing to functions beyond space coding (Scoville and Milner, 1957; Squire, 1982, 1992). This debate has evolved in a place-memory dichotomy for the functional role of the hippocampus until the late 90s, when the initial steps to conciliate memory and spatial navigation were taken (Eichenbaum, 2000a, 2000b; Eichenbaum et al., 1999).

Evidence for contextual dependency on place cell activation (Wood et al., 2000) together with the emergence of the time cells (Eichenbaum, 2014; MacDonald et al., 2011; Pastalkova et al., 2008) – similar to place cells but correlating with time rather than position – suggest that place cells are closely related to memory. Both time and place cells could actually be ‘event cells’ that are associated to the events of being at time X and position Y, respectively. We propose that, as we expand the correlates of place cell activity, we should also expand the investigation into the possible mechanisms that underlie the firing of these cells, which includes studying their firing outside and across the place field.

Still on the differences between inside and outside spikes, when we investigated their relation to the LFP, we found that there was a significant phase-amplitude modulation in CA1 LFPs for the amplitude of the 40-80 Hz band and theta phases in which spikes inside the place field occurred (Figure 4.15A left). This modulation was absent when taking into account theta phases associated with outside spikes (Figure 4.15A right). We note that phase-amplitude modulation exists in LFPs from EC and CA1 (Figure 4.14). Therefore, if the theta phases and gamma amplitudes associated to place cell firing were taken from a random distribution, one would expect to recreate the same pattern of cross-frequency LFP modulation.

However, the phase-amplitude energy plots obtained upon triggering the analysis to timestamps associated to place cell firing are quite distinct from the standard (untriggered) analysis (Figure 4.15). This indicates that CA1 spike times in relation to theta phase and gamma amplitudes do not occur at random, but rather depend on the LFP oscillatory activity.

Although still under debate, it is currently believed that inputs from grid cells in EC are responsible for the emergence of place cells, (Hafting et al., 2005; Moser et al., 2008). These inputs could arrive in CA1 either by a direct way (layer III of EC projecting to CA1), or by an indirect way (layer II projecting to DG and CA3). EC3 inputs to CA1 were shown to be sufficient to maintain spatial firing there (Brun et al., 2002). On the other hand, CA3 would participate in the formation of place fields in novel environments (Nakazawa et al., 2003). In the analysis triggered by inside spikes, the peak modulated frequency in CA1 was ~60 Hz (Figure 4.15), that is, an oscillatory activity at the boundary of the usual definition of LG and HG. Nevertheless, this cross-frequency modulation did not happen for EC3 LFPs, which would be expected by current theories if the modulation were to be associated to HG (Colgin et al., 2009; Schomburg et al., 2014). Thus, the pattern of LFP cross-frequency coupling observed for theta phases associated with the inside spikes could be related to the indirect way, helping place cells to be modulated by CA3 activity. Another possibility is that this cross-frequency coupling would be related to CA1 output targeting EC deep layers. However, maximal gamma amplitude occurred at the peak of the theta oscillation, which is a phase associated with low spiking probability (see Figure 4.3 and Figure 4.10). This theta-modulated gamma could thus be originated from inhibitory interneurons, in accordance to more classical views of gamma generation (Buzsáki et al., 2003). At any event, further investigation is needed to conclude any of these speculations.

Importantly, the inside vs. outside spikes dichotomy proposed at the beginning of this work should be interpreted carefully. Namely, we have shown in later analysis that considering the spikes in a continuous rather than separating them in two groups might be a more proper characterization. However, the small number of spikes outside the place field may diminish the statistical power at the single cell level and, thus, impair a continuous description depending on the analysis protocol. This is

clearly a limitation of the current work, and better designed analyses and experiments should be done for further investigations.

Other limitations of the current work include the unbalanced distribution of place cells across the animals and the arbitrary thresholds used in many definitions. In respect to the former, the high cost and time consumed for each experiment limit the amount of animals available. Unfortunately, this is a common problem of the field, which is usually circumvented by the researchers through the use of other variables as the sample size in statistical analyses (e.g.: number of fields) instead of the number of animals. Concerning the arbitrary choice of threshold values, although they were similar to what was used in literature, their influence on our results should be further investigated.

The novel analyses performed here revealed that spikes concentrate at the ascending phase of theta when gamma amplitude is low, while spikes occur more often at the descending phase during high amplitude of gamma (Figure 4.12 and Figure 4.13), which is to say that periods of low and high amplitude of gamma at a theta timescale mark the beginning and end of the phase precession, respectively. Thus, it is possible that variations of gamma activity within the theta cycle may help to parse chunks of spatial information. We note, however, that gamma amplitude is known to be modulated by theta, irrespective of taking spike times into account (Figure 4.14) (Scheffer-Teixeira et al., 2012). Therefore, whether the relation between gamma and phase precession is an epiphenomenon of theta-gamma coupling, or else if gamma plays an actual role in phase precession per se remains to be elucidated.

6 Conclusions

6 Conclusions

In this work we have studied the spiking activity of place cells, as well as its relation to theta and gamma oscillations in CA1 and EC3. Below we summarize our main findings for each specific objective outlined in the beginning of this dissertation:

Objective 1:

1. Most place fields in the linear track are unidirectional.

2. Firing rate variations as the animal crosses the place field are roughly symmetrical and follow a Gaussian-like shape.

3. The spiking phase of place cells varies as the animal traverses the place field.

Objective 2:

4. Firing rate and spatial information of place cells are not influenced by the mean theta phase of spiking.

5. Firing rate and spatial information of place cells have small negative and positive correlations, respectively, with the strength of theta modulation of spikes.

Objective 3:

6. Spiking theta phase of place cells is dependent on both rate and position.

Objective 4:

7. Theta modulation of place cell spiking activity differs when the animal is inside or outside the place field.

8. Spikes occurring inside the place field, but not outside, oscillate at a faster theta frequency than the LFP theta.

9. Phase precession is asymmetric in relation to the place field center, as defined by the maximal firing rate.

Objective 5:

10. Spikes inside the place field are associated with a 40-80 Hz oscillation in CA1 modulated by theta phase.

11. Within the place field, high and low levels of gamma power are associated with place cell spiking in different theta phases, which characterize the beginning and end of the phase precession.

In all, the bulk of these results suggest that the activity of place cells is related to local field potential oscillations in a variety of ways. Some of the analyses performed here might contribute to the insertion of place cells in a broader scenario of the entorhinal-hippocampal oscillatory circuitry. Our work also adds to the methodological level as we performed new analyses that can be of great use to understand spike-field relations. In particular, we were able to observe the phase precession phenomenon from a different perspective (normalized by the place field distance) and unveil characteristics that remained unnoticed in previous works. Finally, we expect that the present contributions help in the understanding of place cells and the mechanisms and routes of information processing in the hippocampal formation.

References

Andersen, P., Morris, R., Amaral, D., Bliss, T., and O'Keefe, J. (2006). The hippocampus book (Oxford University Press).

Axmacher, N., Henseler, M.M., Jensen, O., Weinreich, I., Elger, C.E., and Fell, J. (2010). Cross-frequency coupling supports multi-item working memory in the human hippocampus. Proc. Natl. Acad. Sci. *107*, 3228–3233.

Belchior, H., Lopes-dos-Santos, V., Tort, A.B., and Ribeiro, S. (2014). Increase in hippocampal theta oscillations during spatial decision making. Hippocampus *24*, 693–702.

Berens, P. (2009). CircStat: a MATLAB toolbox for circular statistics. J Stat Softw *31*, 1–21.

Bieri, K.W., Bobbitt, K.N., and Colgin, L.L. (2014). Slow and Fast Gamma Rhythms Coordinate Different Spatial Coding Modes in Hippocampal Place Cells. Neuron *82*, 670–681.

Bland, B.H., and Oddie, S.D. (2001). Theta band oscillation and synchrony in the hippocampal formation and associated structures: the case for its role in sensorimotor integration. Behav. Brain Res. *127*, 119–136.

Bragin, A., Jandó, G., Nádasdy, Z., Hetke, J., Wise, K., and Buzsáki, G. (1995). Gamma (40-100 Hz) oscillation in the hippocampus of the behaving rat. J. Neurosci. *15*, 47–60.

Brosch, M., Budinger, E., and Scheich, H. (2002). Stimulus-related gamma oscillations in primate auditory cortex. J. Neurophysiol. *87*, 2715–2725.

Brun, V.H., Otnæss, M.K., Molden, S., Steffenach, H.-A., Witter, M.P., Moser, M.-B., and Moser, E.I. (2002). Place cells and place recognition maintained by direct entorhinal-hippocampal circuitry. Science *296*, 2243–2246.

Bunsey, M., and Eichenbaum, H. (1996). Conservation of hippocampal memory function in rats and humans. Nature *379*, 255–257.

Buzsáki, G. (2005). Theta rhythm of navigation: link between path integration and landmark navigation, episodic and semantic memory. Hippocampus *15*, 827–840.

Buzsáki, G., Lai-Wo S., L., and Vanderwolf, C.H. (1983). Cellular bases of hippocampal EEG in the behaving rat. Brain Res. Rev. *6*, 139–171.

Buzsáki, G., Buhl, D.L., Harris, K.D., Csicsvari, J., Czeh, B., and Morozov, A. (2003). Hippocampal network patterns of activity in the mouse. Neuroscience *116*, 201–211.

Buzsáki, G., Anastassiou, C.A., and Koch, C. (2012). The origin of extracellular fields and currents—EEG, ECoG, LFP and spikes. Nat. Rev. Neurosci. *13*, 407–420.

Canolty, R.T., and Knight, R.T. (2010). The functional role of cross-frequency coupling. Trends Cogn. Sci. *14*, 506–515.

Cei, A., Girardeau, G., Drieu, C., El Kanbi, K., and Zugaro, M. (2014). Reversed theta sequences of hippocampal cell assemblies during backward travel. Nat. Neurosci.

Colgin, L.L., Denninger, T., Fyhn, M., Hafting, T., Bonnevie, T., Jensen, O., Moser, M.-B., and Moser, E.I. (2009). Frequency of gamma oscillations routes flow of information in the hippocampus. Nature *462*, 353–357.

Corkin, S. (1968). Acquisition of motor skill after bilateral medial temporal-lobe excision. Neuropsychologia *6*, 255–265.

Csicsvari, J., Jamieson, B., Wise, K.D., and Buzsáki, G. (2003). Mechanisms of gamma oscillations in the hippocampus of the behaving rat. Neuron *37*, 311–322.

Desmedt, J.E., and Tomberg, C. (1994). Transient phase-locking of 40 Hz electrical oscillations in prefrontal and parietal human cortex reflects the process of conscious somatic perception. Neurosci. Lett. *168*, 126–129.

Eichenbaum, H. (2000a). A cortical–hippocampal system for declarative memory. Nat. Rev. Neurosci. *1*, 41–50.

Eichenbaum, H. (2000b). Hippocampus: Mapping or memory? Curr. Biol. *10*, R785–R787.

Eichenbaum, H. (2014). Time cells in the hippocampus: a new dimension for mapping memories. Nat. Rev. Neurosci. *15*, 732–744.

Eichenbaum, H., Fagan, A., and Cohen, N.J. (1986). Normal olfactory discrimination learning set and facilitation of reversal learning after medial-temporal damage in rats: implications for an account of preserved learning abilities in amnesia. J. Neurosci. *6*, 1876–1884.

Eichenbaum, H., Mathews, P., and Cohen, N.J. (1989). Further studies of hippocampal representation during odor discrimination learning. Behav. Neurosci. *103*, 1207–1216.

Eichenbaum, H., Dudchenko, P., Wood, E., Shapiro, M., and Tanila, H. (1999). The hippocampus, memory, and place cells: is it spatial memory or a memory space? Neuron *23*, 209–226.

Fell, J., Fernandez, G., Klaver, P., Elger, C.E., and Fries, P. (2003). Is synchronized neuronal gamma activity relevant for selective attention? Brain Res. Rev. *42*, 265–272.

Fox, S.E., and Ranck Jr, J.B. (1981). Electrophysiological characteristics of hippocampal complex-spike cells and theta cells. Exp. Brain Res. *41*, 399–410.

Fox, S.E., Wolfson, S., and Ranck Jr, J.B. (1986). Hippocampal theta rhythm and the firing of neurons in walking and urethane anesthetized rats. Exp. Brain Res. *62*, 495–508.

Freeman, W.J. (1978). Spatial properties of an EEG event in the olfactory bulb and cortex. Electroencephalogr. Clin. Neurophysiol. *44*, 586–605.

Fries, P., Reynolds, J.H., Rorie, A.E., and Desimone, R. (2001). Modulation of oscillatory neuronal synchronization by selective visual attention. Science *291*, 1560–1563.

Fuster, J.M. (2001). The Prefrontal Cortex—An Update: Time Is of the Essence. Neuron *30*, 319–333.

Geisler, C., Robbe, D., Zugaro, M., Sirota, A., and Buzsáki, G. (2007). Hippocampal place cell assemblies are speed-controlled oscillators. Proc. Natl. Acad. Sci. *104*, 8149–8154.

Geisler, C., Diba, K., Pastalkova, E., Mizuseki, K., Royer, S., and Buzsáki, G. (2010). Temporal delays among place cells determine the frequency of population theta oscillations in the hippocampus. Proc. Natl. Acad. Sci. *107*, 7957–7962.

Gray, C.M., and Singer, W. (1989). Stimulus-specific neuronal oscillations in orientation columns of cat visual cortex. Proc. Natl. Acad. Sci. *86*, 1698–1702.

Gruber, T., Müller, M.M., Keil, A., and Elbert, T. (1999). Selective visual-spatial attention alters induced gamma band responses in the human EEG. Clin. Neurophysiol. *110*, 2074–2085.

Hafting, T., Fyhn, M., Molden, S., Moser, M.-B., and Moser, E.I. (2005). Microstructure of a spatial map in the entorhinal cortex. Nature *436*, 801–806.

Harris, K.D., Henze, D.A., Csicsvari, J., Hirase, H., and Buzsáki, G. (2000). Accuracy of tetrode spike separation as determined by simultaneous intracellular and extracellular measurements. J. Neurophysiol. *84*, 401–414.

Harris, K.D., Henze, D.A., Hirase, H., Leinekugel, X., Dragoi, G., Czurkó, A., and Buzsáki, G. (2002). Spike train dynamics predicts theta-related phase precession in hippocampal pyramidal cells. Nature *417*, 738–741.

Huxter, J., Burgess, N., and O'Keefe, J. (2003). Independent rate and temporal coding in hippocampal pyramidal cells. Nature *425*, 828–832.

Jensen, O., and Colgin, L.L. (2007). Cross-frequency coupling between neuronal oscillations. Trends Cogn. Sci. *11*, 267–269.

Jung, M.W., Wiener, S.I., and McNaughton, B.L. (1994). Comparison of spatial firing characteristics of units in dorsal and ventral hippocampus of the rat. J. Neurosci. *14*, 7347–7356.

Kramis, R., Vanderwolf, C.H., and Bland, B.H. (1975). Two types of hippocampal rhythmical slow activity in both the rabbit and the rat: Relations to behavior and effects of atropine, diethyl ether, urethane, and pentobarbital. Exp. Neurol. *49*, 58–85.

Lebedev, M.A., and Nelson, R.J. (1995). Rhythmically firing (20–50 Hz) neurons in monkey primary somatosensory cortex: activity patterns during initiation of vibratory-cued hand movements. J. Comput. Neurosci. *2*, 313–334.

Lima, B., Singer, W., and Neuenschwander, S. (2011). Gamma Responses Correlate with Temporal Expectation in Monkey Primary Visual Cortex. J. Neurosci. *31*, 15919–15931.

Lubenov, E.V., and Siapas, A.G. (2009). Hippocampal theta oscillations are travelling waves. Nature *459*, 534–539.

MacDonald, C.J., Lepage, K.Q., Eden, U.T., and Eichenbaum, H. (2011). Hippocampal “Time Cells” Bridge the Gap in Memory for Discontiguous Events. Neuron *71*, 737–749.

McNaughton, B.L., Barnes, C.A., and O’keefe, J. (1983). The contributions of position, direction, and velocity to single unit activity in the hippocampus of freely-moving rats. Exp. Brain Res. *52*, 41–49.

Mehta, M.R., Quirk, M.C., and Wilson, M.A. (2000). Experience-Dependent Asymmetric Shape of Hippocampal Receptive Fields. Neuron *25*, 707–715.

Mehta, M.R., Lee, A.K., and Wilson, M.A. (2002). Role of experience and oscillations in transforming a rate code into a temporal code. Nature *417*, 741–746.

Milner, B., Corkin, S., and Teuber, H.-L. (1968). Further analysis of the hippocampal amnesic syndrome: 14-year follow-up study of HM. Neuropsychologia *6*, 215–234.

Mishkin, M. (1978). Memory in monkeys severely impaired by combined but not by separate removal of amygdala and hippocampus.

Mizuseki, K., Sirota, A., Pastalkova, E., and Buzsáki, G. (2009). Theta oscillations provide temporal windows for local circuit computation in the entorhinal-hippocampal loop. Neuron *64*, 267–280.

Mizuseki, K., Sirota, A., Pastalkova, E., Diba, K., and Buzsáki, G. (2013). Multiple single unit recordings from different rat hippocampal and entorhinal regions while the animals were performing multiple behavioral tasks. CRCNS Org.

Mizuseki, K., Diba, K., Pastalkova, E., Teeters, J., Sirota, A., and Buzsáki, G. (2014). Neurosharing: large-scale data sets (spike, LFP) recorded from the hippocampal-entorhinal system in behaving rats. F1000Research *3*.

Morris, R.G.M., Garrud, P., Rawlins, J.N.P., and O’Keefe, J. (1982). Place navigation impaired in rats with hippocampal lesions. Nature *297*, 681–683.

Moser, E.I., Kropff, E., and Moser, M.-B. (2008). Place cells, grid cells, and the brain's spatial representation system. Annu Rev Neurosci *31*, 69–89.

Muller, R.U., and Kubie, J.L. (1987). The Effects of Changes in the Environment on the Spatial Firing of Hippocampal Complex-Spike Cells.

Muller, R.U., Kubie, J.L., and Ranck Jr, J.B. (1987). Spatial firing patterns of hippocampal complex-spike cells in a fixed environment. J Neurosci *7*, 1935–1950.

Muller, R.U., Bostock, E., Taube, J.S., and Kubie, J.L. (1994). On the directional firing properties of hippocampal place cells. J. Neurosci. *14*, 7235–7251.

Nadel, L., and Moscovitch, M. (1997). Memory consolidation, retrograde amnesia and the hippocampal complex. Curr. Opin. Neurobiol. *7*, 217–227.

Nakazawa, K., Sun, L.D., Quirk, M.C., Rondi-Reig, L., Wilson, M.A., and Tonegawa, S. (2003). Hippocampal CA3 NMDA Receptors Are Crucial for Memory Acquisition of One-Time Experience. Neuron *38*, 305–315.

O'Keefe, J., and Conway, D.H. (1978). Hippocampal place units in the freely moving rat: Why they fire where they fire. Exp. Brain Res. *31*, 573–590.

O'Keefe, J., and Dostrovsky, J. (1971). The hippocampus as a spatial map. Preliminary evidence from unit activity in the freely-moving rat. Brain Res. *34*, 171–175.

O'Keefe, J., and Nadel, L. (1978). The hippocampus as a cognitive map (Clarendon Press Oxford).

O'Keefe, J., and Recce, M.L. (1993). Phase relationship between hippocampal place units and the EEG theta rhythm. Hippocampus *3*, 317–330.

O'Keefe, J., and Speakman, A. (1987). Single unit activity in the rat hippocampus during a spatial memory task. Exp. Brain Res. *68*, 1–27.

O'Keefe, J., Nadel, L., Keightley, S., and Kill, D. (1975). Fornix lesions selectively abolish place learning in the rat. Exp. Neurol. *48*, 152–166.

O'Keefe, J., Burgess, N., Donnett, J.G., Jeffery, K.J., and Maguire, E.A. (1998). Place cells, navigational accuracy, and the human hippocampus. Philos. Trans. R. Soc. Lond. B. Biol. Sci. *353*, 1333–1340.

Olton, D.S., Walker, J.A., and Gage, F.H. (1978a). Hippocampal connections and spatial discrimination. Brain Res. *139*, 295–308.

Olton, D.S., Branch, M., and Best, P.J. (1978b). Spatial correlates of hippocampal unit activity. Exp. Neurol. *58*, 387–409.

Pastalkova, E., Itskov, V., Amarasingham, A., and Buzsáki, G. (2008). Internally Generated Cell Assembly Sequences in the Rat Hippocampus. Science *321*, 1322–1327.

Quirk, G.J., Muller, R.U., and Kubie, J.L. (1990). The firing of hippocampal place cells in the dark depends on the rat's recent experience. J. Neurosci. *10*, 2008–2017.

Ranck Jr, J.B. (1984). Head direction cells in the deep cell layer of dorsal presubiculum in freely moving rats. In Soc Neurosci Abstr,.

Redish, A.D., Battaglia, F.P., Chawla, M.K., Ekstrom, A.D., Gerrard, J.L., Lipa, P., Rosenzweig, E.S., Worley, P.F., Guzowski, J.F., McNaughton, B.L., et al. (2001). Independence of firing correlates of anatomically proximate hippocampal pyramidal cells. J Neurosci *21*, RC134.

Scheffer-Teixeira, R., Belchior, H., Caixeta, F.V., Souza, B.C., Ribeiro, S., and Tort, A.B.L. (2012). Theta Phase Modulates Multiple Layer-Specific Oscillations in the CA1 Region. Cereb. Cortex *22*, 2404–2414.

Schomburg, E.W., Fernández-Ruiz, A., Mizuseki, K., Berényi, A., Anastassiou, C.A., Koch, C., and Buzsáki, G. (2014). Theta Phase Segregation of Input-Specific Gamma Patterns in Entorhinal-Hippocampal Networks. Neuron *84*, 470–485.

Scoville, W.B., and Milner, B. (1957). Loss of recent memory after bilateral hippocampal lesions. J. Neurol. Neurosurg. Psychiatry *20*, 11.

Senior, T.J., Huxter, J.R., Allen, K., O'Neill, J., and Csicsvari, J. (2008). Gamma Oscillatory Firing Reveals Distinct Populations of Pyramidal Cells in the CA1 Region of the Hippocampus. J. Neurosci. *28*, 2274–2286.

Skaggs, W.E., McNaughton, B.L., Gothard, K.M., and Markus, E.J. (1993). An information-theoretic approach to deciphering the hippocampal code. In In, (Citeseer),.

Sławińska, U., and Kasicki, S. (1998). The frequency of rat's hippocampal theta rhythm is related to the speed of locomotion. Brain Res. *796*, 327–331.

Squire, L.R. (1982). The neuropsychology of human memory. Annu. Rev. Neurosci. *5*, 241–273.

Squire, L.R. (1992). Memory and the hippocampus: a synthesis from findings with rats, monkeys, and humans. Psychol. Rev. *99*, 195.

Squire, L.R., and Zola-Morgan, S. (1991). The medial temporal lobe memory system. Science *253*, 1380–1386.

Taube, J.S., Muller, R.U., and Ranck, J.B. (1990). Head-direction cells recorded from the postsubiculum in freely moving rats. I. Description and quantitative analysis. J. Neurosci. *10*, 420–435.

Tort, A.B., Kramer, M.A., Thorn, C., Gibson, D.J., Kubota, Y., Graybiel, A.M., and Kopell, N.J. (2008). Dynamic cross-frequency couplings of local field potential oscillations in rat striatum and hippocampus during performance of a T-maze task. Proc. Natl. Acad. Sci. U. S. A. *105*, 20517.

Tort, A.B., Komorowski, R.W., Manns, J.R., Kopell, N.J., and Eichenbaum, H. (2009). Theta–gamma coupling increases during the learning of item–context associations. Proc. Natl. Acad. Sci. *106*, 20942–20947.

Tort, A.B.L., Komorowski, R., Eichenbaum, H., and Kopell, N. (2010). Measuring Phase-Amplitude Coupling Between Neuronal Oscillations of Different Frequencies. J. Neurophysiol. *104*, 1195–1210.

Vanderwolf, C.H. (1969). Hippocampal electrical activity and voluntary movement in the rat. Electroencephalogr. Clin. Neurophysiol. *26*, 407–418.

Victor, M., and Agamanolis, D. (1990). Amnesia due to lesions confined to the hippocampus: A clinical-pathologic study. J. Cogn. Neurosci. *2*, 246–257.

Winson, J. (1972). Interspecies differences in the occurrence of theta. Behav. Biol. *7*, 479–487.

Winson, J. (1978). Loss of hippocampal theta rhythm results in spatial memory deficit in the rat. Science *201*, 160–163.

Witter, M.P. (1992). Organization of the entorhinal-hippocampal system: a review of current anatomical data. Hippocampus *3*, 33–44.

Wood, E.R., Dudchenko, P.A., Robitsek, R.J., and Eichenbaum, H. (2000). Hippocampal Neurons Encode Information about Different Types of Memory Episodes Occurring in the Same Location. Neuron *27*, 623–633.

Zola-Morgan, S.M., and Squire, L.R. (1990). The primate hippocampal formation: evidence for a time-limited role in memory storage. Science *250*, 288–290.

Zola-Morgan, S., and Squire, L.R. (1984). Preserved learning in monkeys with medial temporal lesions: Sparing of motor and cognitive skills. J. Neurosci. *4*, 1072–1085.

Zola-Morgan, S., Squire, L.R., and Amaral, D.G. (1986). Human amnesia and the medial temporal region: enduring memory impairment following a bilateral lesion limited to field CA1 of the hippocampus. J. Neurosci. *6*, 2950–2967.

Zola-Morgan, S., Squire, L.R., and Amaral, D.G. (1989). Lesions of the amygdala that spare adjacent cortical regions do not impair memory or exacerbate the impairment following lesions of the hippocampal formation. J. Neurosci. *9*, 1922–1936.